Diploma thesis

Function and Expression of Cancer Mutations of the KCNJ3 Gene

submitted by

Ahmed Hatab

for obtaining the academic degree

Doctor medicinae universae

(Dr. med. univ.)

at the

Medical University of Graz

conducted at the

Division of Medical Physics and Biophysics

under the supervision of

Ao.Univ.-Prof. Dr.phil. Wolfgang Schreibmayer

Ms. Astrid Gorischek

Graz, 21/02/2023

Declaration of Academic Integrity

I hereby declare that the following diploma thesis has been written only by the undersigned and without any assistance from third parties. Furthermore, I confirm that no sources have been used in the preparation of this thesis other than those indicated in the thesis itself.

Graz, 21/02/2023 *Ahmed Hatab m.p.*

Acknowledgements

I would like to thank my family for always being there for me and would also like to give special thanks to my diploma thesis supervisors Prof. Wolfgang Schreibmayer and Ms. Astrid Gorischek and every staff member of the Gottfried Schatz Research Center for Cell Signaling, Metabolism and Ageing who gave me assistance working in the lab and helping me to produce the best quality possible to complete my diploma thesis.

Table of Contents

Abbreviations

Δ

ΔF: Difference in fluorescence intensity between the membrane and the background

C

cLSM: Confocal laser scan microscopy

E

eGFP: Enhanced green fluorecent protein

G

GDC: Genomic Data Commons
GIRK1: G protein-activated inward rectifier potassium channel 1
GIRK2: G protein-activated inward rectifier potassium channel 2
GIRK3: G protein-activated inward rectifier potassium channel 3
GIRK4: G protein-activated inward rectifier potassium channel 4
GIRK5: G protein-activated inward rectifier potassium channel 5

I

I_{total}: Total electric current = IHK + IACh

K

KCNJ3: Potassium Inwardly Rectifying Channel Subfamily J Member 3
KCNJ5: Potassium Inwardly Rectifying Channel Subfamily J Member 5
KCNJ6: Potassium Inwardly Rectifying Channel Subfamily J Member 6
KCNJ9: Potassium Inwardly Rectifying Channel Subfamily J Member 9
Kir3.1-4: Synonyms for GIRK 1-4

M

M2R: muscarinic acetylcholine receptor M2

N

NCI: National Cancer Institute

P

PMTs: Photomultiplier tubes

S

SSM: Simple somatic mutation

T

TEVC: Two Electrode Voltage clamp

W

WT: Wild type

Table of Figures

List of Tables

Zusammenfassung

Einführung:

Recherchen im GDC Data Portal des NCI in 13.714 primären Tumoren ergaben 305 primäre bösartige Tumore, welche insgesamt 321 somatischen Mutationen des KCNJ3 Gens enthielten. In Tumoren von Uterus, Haut und Lunge wurden somatische KCNJ3-Mutationen am häufigsten gefunden https://portal.gdc.cancer. Wir konzentrierten uns auf 15 Missense-Mutationen in einem Abschnitt, der das Leitmotif der Ionenselektivität und die für die Ionenselektivität wesentliche P-Helix der Porenstruktur zwischen der ersten und der zweiten Transmembranhelix umfasst (Nishida, Cadene et al. 2007).

Ziel, Material und Methoden:

Der Schwerpunkt dieser Diplomarbeit liegt auf der Untersuchung möglicher Auswirkungen von KCNJ3-Mutationen auf (a) Proteinexpression, (b) Ionenkanal-Gating, (c) Ionenselektivität und (d) Untereinheitsanordnung von GIRK-Kanälen. Die elektrophysiologische Charakterisierung von GIRK-Kanälen, die in Oozyten von *Xenopus laevis*, exprimiert wurden, wurde unter Verwendung der TEVC erzielt. Die Menge an exprimiertem Protein wurde unter Verwendung vom cLSM quantifiziert.

Ergebnisse:

Die in dieser Arbeit untersuchten Mutationen zeigten Phänotypen, die in drei Hauptgruppen eingeteilt werden konnten: (i) normale/reduzierte Expression zusammen mit verminderter/fehlender Funktion (S132Y, F136L, E139K, G145A, R149Q, R149P, G178D, S185Y, Q186R) (ii) normale/erhöhte Expression zusammen mit erhöhter Funktion (E140M, A142T, M184I) und (iii) geringe Expression, jedoch erhöhte Funktion (I151N, G158S).

Diskussion:

Es wurde beobachtet, dass keine der analysierten Mutationen zu funktionierenden homomeren Ionenkanälen führen kann. Die geringfügigen Amplituden von Strömen, die an vermeintlich homooligomeren GIRK Kanälen beobachtet wurden, wurden wahrscheinlich durch nicht vollständiges Antisense-Oligonukleotid- Gen-Knockdown der endogenen GIRK5-Untereinheit verursacht. Wir schlagen eine mögliche Rolle der Gruppen (ii) und (iii) bei der Entwicklung und dem Fortschreiten von malignen Tumoren, besonders in Tumortypen, in denen häufig somatische KCNJ3-Mutationen auftreten vor. Weitere Studien zu menschlichem Krebs, speziell zu seiner Proliferation und Differenzierung werden notwendig sein, um festzustellen, ob somatische Mutationen im KCNJ3-Gen für klinische Anwendungen wichtig sein könnten.

Abstract

Introduction:

Searching the Genomic Data Commons (GDC) Data Portal of the National Cancer Institute (NCI) revealed 305 cancer cases out of 13,714 cases of primary malignant tumors that contained 321 somatic mutations of the KCNJ3 gene. The uterine, skin, and lung tumors with KCNJ3 somatic mutations were the most common sites for these mutations https://portal.gdc.cancer. We concentrated on 15 missense mutations in a section that comprises the ion selectivity fingerprint and the P-helix, which are essential for ion selectivity. This region is located between the first and second transmembrane helix (Nishida, Cadene et al. 2007).

Aim, material and methods:

The focus of this diploma thesis is to investigate potential effects of KCNJ3 mutations on (a) protein expression, (b) ion channel gating, (c) ion selectivity, and (d) subunit assembly of GIRK channels. Electrophysiological characterization of GIRK channels expressed in Xenopus laevis oocytes, both wild-type and mutant, was achieved by using the Two Electrode Voltage clamp (TEVC). The level of expressed protein was evaluated utilizing confocal laser scan microscopy (cLSM).

Results:

The mutations investigated in this thesis showed phenotypes that could be classified into three main groups: (i) normal/reduced expression along with decreased/absent function (S132Y, F136L, E139K, G145A, R149Q, R149P, G178D, S185Y, Q186R) (ii) normal/increased expression along with increased function (E140M, A142T, M184I) and (iii) low expression however increased function (I151N, G158S).

Discussion:

It has been observed that none of the analyzed mutations can result in functioning homomeric ion channels, and any trace amounts of currents that were seen have been caused by a lack of antisense oligonucleotide silencing of the endogenous GIRK5 subunit. We propose that groups (ii) and (iii) may have a role in the development and progression of malignancies, especially in tissues where somatic KCNJ3 mutations arise frequently. Further studies on human cancer, cancer proliferation, and differentiation will be necessary to determine if somatic mutations in the KCNJ3 gene might indeed be important in clinical applications.

Information from already made publications

The data and results of the prevalent diploma thesis have been already published in: Pelzmann B, Hatab A, Scheruebel S, Langthaler S, Rienmueller T, Sokolowski A, Gorischek A, Platzer D, Zorn-Pauly K, Jahn SW, Bauernhofer T and Schreibmayer W (2022). Consequences of somatic mutations of GIRK1 detected in primary malign tumors on expression and function of G-protein activated, inwardly rectifying, K^+ channels. Front. Oncol. 12:998907. https://doi.org/10.3389/fonc.2022.998907.

Figures and tables, to which my contribution was substantial, were selected from the publication above. These are shown in this thesis and are marked as citation.

1 Introduction

1.1 Biology of Cancer and the role of somatic mutations:

Within the last 3 to 4 decades of cancer research, a countless number of studies have shown several and complex ways how cancer cells can develop. The vast majority if not all agree, that the development of neoplastic cells is a multistep process, which involves the dysfunction of regulation of cell proliferation and homeostasis. One of the most prominent treatises (Hanahan, Weinberg 2000) proposes, that most, if not all, cancer cells are characterized by six distinctive biological capabilities, acquired during the process of carcinogenesis, now known as the six hallmarks of cancer (Hanahan, Weinberg 2000). These six hallmarks of cancer are described as follows (Figure 1): (i) Self-sufficiency in growth signals, (ii) Insensitivity to anti-growth signals, (iii) Tissue invasion and metastasis, (iv) Limitless replicative potential, (v) Sustained angiogenesis and (vi) Evading apoptosis (Hanahan, Weinberg 2000). Later on (Hanahan, Weinberg 2011) extend this scheme and suggest (Figure 2) that two additional "emerging" cancer hallmarks, i.e. (vii) Deregulation of cellular energetics and (viii) Avoiding immune destruction represent also important acquired features of malignant cancer cells. In addition, both "core" and "emerging" hallmarks are proposed to be facilitated by two consequential characteristics, i.e. (a) genome instability and mutation and (b) Tumor-promoting inflammation (Hanahan, Weinberg 2011).

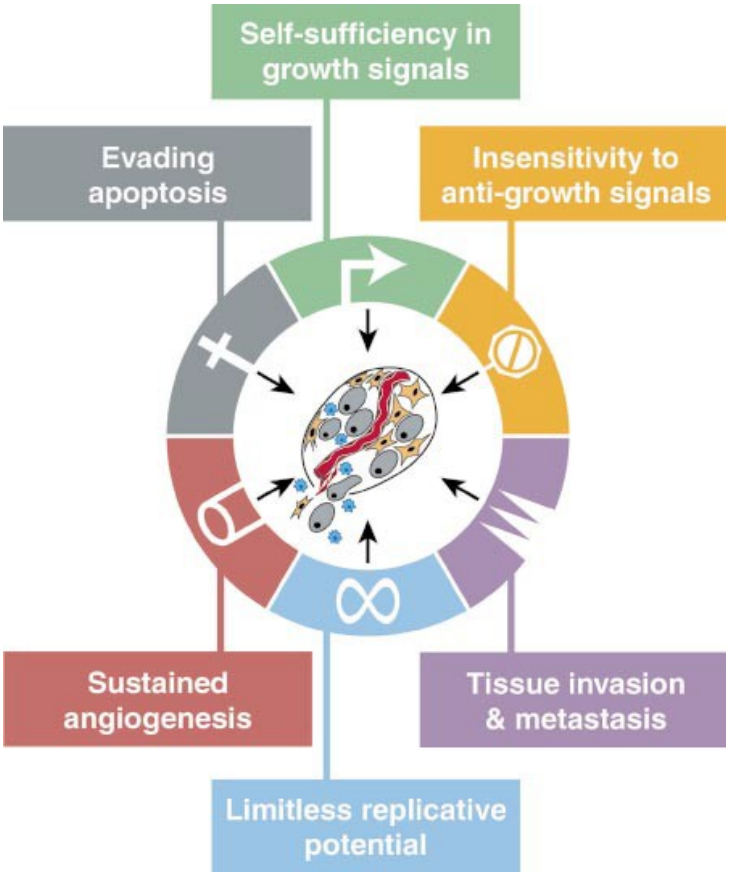

Figure 1: Acquired Capabilities of Cancer
From: (Hanahan, Weinberg 2000).

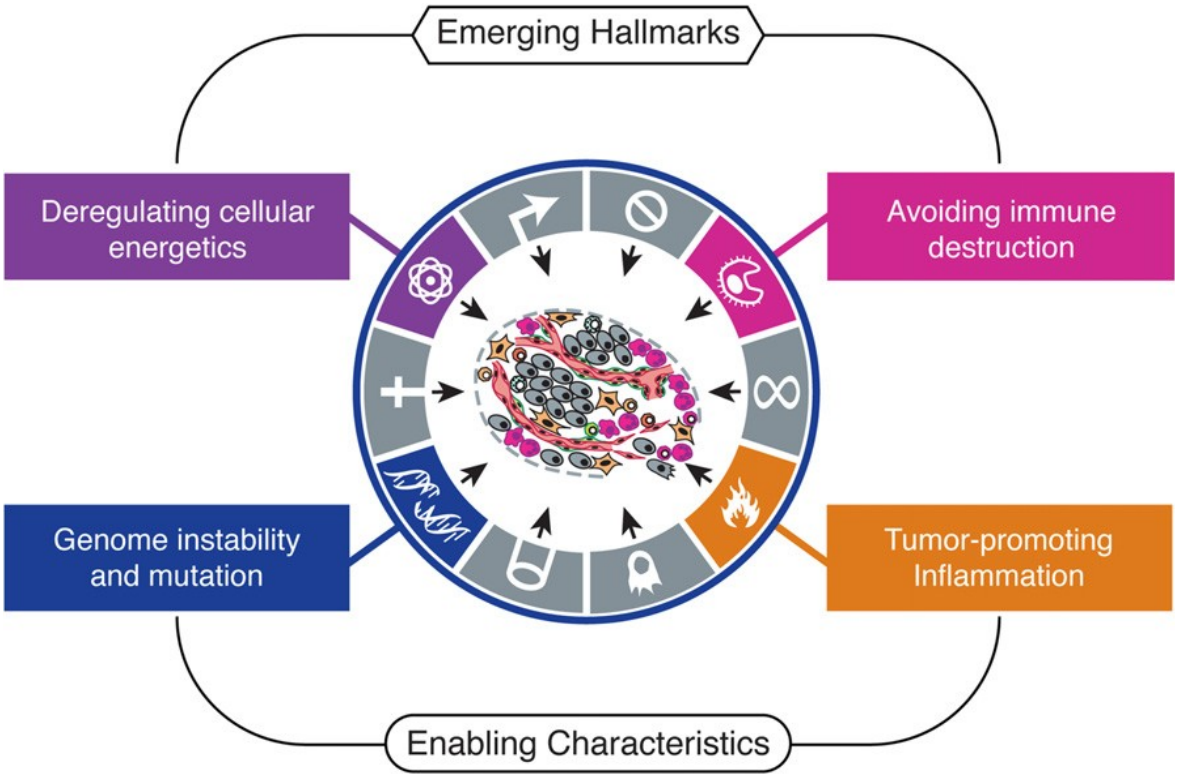

Figure 2: Emerging Hallmarks and Enabling Characteristics

From (Hanahan, Weinberg 2011).

Inevitable for providing sufficient lifespans for eucaryotic cells are systems that maintain genomic integrity, that monitor, detect and reverse or resolve defects and/or mutations in the DNA, caused by ionizing radiation and/or cancerogenic chemical compounds. These mechanisms save the cells from transition to precancerous lesions and finally from becoming malignant (Loeb 1991, Salk, Fox et al. 2010, Negrini, Gorgoulis et al. 2010). In order to undergo carcinogenesis and malignant transformation, malfunction of one or several components of the surveillance systems that are responsible to check any damage in the genomic integrity, is required (Sigal, Rotter 2000, Kastan 2008, Jackson, Bartek 2009). Defects in these entities, that are in charge of the DNA maintenance also known as the "caretakers" of the genome, have been documented to increase the mutability of normal cells (Kinzler, Vogelstein 1997, Levine 1997). One of the most well-known components of the DNA maintenance system is the p53 tumor suppressor protein known as "guardian of the genome" (Lane 1992). The function of p53 is now well understood, it plays an important role in regulating the cell cycle in response to damage of the DNA, which either causes cell cycle arrest or apoptosis (in case the damage is too severe or irreversible for it to be repaired; (Levine 1997)). Recent evidence suggests, however, that apoptosis can contribute to the instability of the genome, as apoptotic cell bodies that

comprise the damaged genome, can be incorporated through phagocytosis by the neighboring cells into their genetic information (Holmgren, Szeles et al. 1999).

Numerous research also uncovered that genome instability can be achieved through epigenetic mechanisms such as histone modifications and DNA methylation, by which it can inactivate some tumor suppressor genes (Esteller 2007, Jones, Baylin 2007, Berdasco, Esteller 2010). Another mechanism that can play a role in the genome instability, is the loss of the function of telomerase, which can lead to unlimited replicative potential (Artandi, DePinho 2010).

Facilitated via technological advances in molecular genetic analysis of cancer cell's DNA, researchers were able to uncover different types of mutations that affect genome stability during tumor development and progression. Comparative genomic hybridization is one example of genetic analysis, in which one can analyze a copy number variation of one DNA sample and compare it with another reference sample. Such studies allowed researchers to provide clear evidence, that loss or gain of gene copies in a normal cell is more likely to acquire neoplastic characteristics, enabling the cell to progress towards a tumor cell (Korkola, Gray 2010).

Modern DNA sequencing methods allow us to reveal somatic mutations in different types tumors, clearly documenting genome instability and mutations as an enabling characteristic for tumor development and progression in normal cells (Hanahan, Weinberg 2011).

1.2 Role of KCNJ3 gene in cancer:

Early evidence on the important role of ion channels in tumorigenesis came through observation of cancer cell lines with abnormal expression of ion channels and the inhibition of tumor cells progression via pharmacological ion channel blockers (Yamashita, Hamada et al. 1987, Lee, Deutsch et al. 1988, Pancrazio, Viglione et al. 1989, Batra, Alenfall 1991, Taylor, Simpson 1992, Pancrazio, Tabbara et al. 1993). Since these early observations, the interest of the scientific community in ion channels and their possible role in tumorigenesis has significantly increased throughout the years. As plethora of evidence and confirmations of the important role of ion channels in tumorigenesis has been uncovered, which finally led to the description of oncochannelopathies as one of the major characteristics of cancer hallmarks (Prevarskaya, Skryma et al. 2010, Huber 2013, Litan, Langhans 2015).

In this diploma thesis our main aim is to study the function of cancer mutations of KCNJ3 gene. KCNJ3 gene is one of the four genes (KCNJ3, KCNJ5, KCNJ6, KCNJ9) that encode subunits of the human G-protein-activated inward rectifier potassium (K^+) channel

subfamily (Kir3.1-4; GIRK 1-4). KCNJ3 gene encodes the GIRK1 protein. The GIRK1-4 subfamily proteins form a homo- or a hetero-tetrameric ion channel complex, which can be found in the plasma membrane. GIRK ion channels play an important role in the regulation of cellular excitability and are activated via extracellular signals, e.g., hormones and neurotransmitters (Lüscher, Slesinger 2010). Evidence from recent studies suggested a correlation between overexpression of the KCNJ3 gene product and progression of non-small lung cancer (Takanami, Inoue et al. 2004), Another study reported upregulation of GIRK1 protein in pancreatic adenocarcinomas (Brevet, Fucks et al. 2009). Several studies have shown a correlation between upregulation of the KCNJ3 gene and breast cancer progression. One study detected overexpression of the KCNJ3 mRNA in primary invasive breast carcinomas in comparison with the corresponding normal healthy breast tissue and also a positive correlation of KCNJ3 mRNA expression with the numbers of metastatic lymph nodes (Stringer, Cooper et al. 2001). Another study confirmed the positive correlation ofGIRK1 protein expression in breast tumor in comparison to normal breast tissue and a higher mortality rate in patients (Brevet, Ahidouch et al. 2008). Furthermore, another study showed enhanced motility, invasiveness, and angiogenesis of KCNJ3 overexpressing in MCF-7 breast cancer cells compared with controls which further emphasize the importance of KCNJ3 in breast cancer (Rezania, Kammerer et al. 2016). KCNJ3 was also noticed to be upregulated in breast cancer with positive estrogen receptor but a decrease of expression in the p53 mutant breast cancer (Ko, Ko et al. 2013). Later on it was confirmed, that there is an overexpression of KCNJ3 in breast tumors in comparison to normal breast tissue and a significantly upregulation of the KCNJ3 mRNA in estrogen positive receptor breast cancer, demonstrating that KCNJ3 expression can be used as an independent prognostic marker and patients with positive estrogen receptor and a high KCNJ3 mRNA expression levels exerting worse survival outcome compared to low levels of KCNJ3 gene expression (Kammerer, Sokolowski et al. 2016). Considering these findings, the subject of whether somatic mutations of the KCNJ3 gene have been found in malignant tumors and whether these changes are functional and affect expression and function, was one that sparked our curiosity. Hence, the aim of the prevalent diploma thesis was to study potential impacts of KCNJ3 mutations on (a) protein expression, (b) ion channel gating, (c) ion selectivity and (d) subunit assembly of GIRK channels. GIRK channels expressed in Xenopus laevis oocytes, both wild-type and mutant, were subjected to electrophysiological characterization. Confocal laser scan microscopy was used to measure the amount of protein expressed.

1.3 Identification of KCNJ3 mutations in cancer base:

Data provided from the National Cancer Institute (NCI) Genomic Data Commons (GDC) Data Portal reveal that from over 86,000 cancer cases and over 2,700,000 mutations, there are about 605 cancer cases and 689 mutations affecting the KCNJ subfamily genes 305 malignant primary tumors and 321 somatic mutations of the KCNJ3 subunit gene were detected. KCNJ3 somatic mutations were most frequently found in tumors from the uterus, skin, and lung are shown in Table 1. (Data from Dec. 2022.). In Figure 3 the incidence of mutations of the four genes that constitute GIRK channels (KCNJ3, KCNJ5, KCNJ6, KCNJ9) in relation to selected genes that are frequently mutated in cancer cells is shown. Figure 4 displays the incidence of cases with mutated KCNJ family gene in comparison within each other, which shows 50% of the cases affected with mutated KCNJ3 gene. A total of 305 cases of somatic KCNJ3 gene mutations have been identified out of 13,714 cases of primary malignant tumors of any origin across the GDC see Table 3 for a complete list of the mutations identified, where the most frequent somatic mutations in KCNJ3 were found in lung, cutaneous, and uterine cancers. (Data from Dec. 2022).

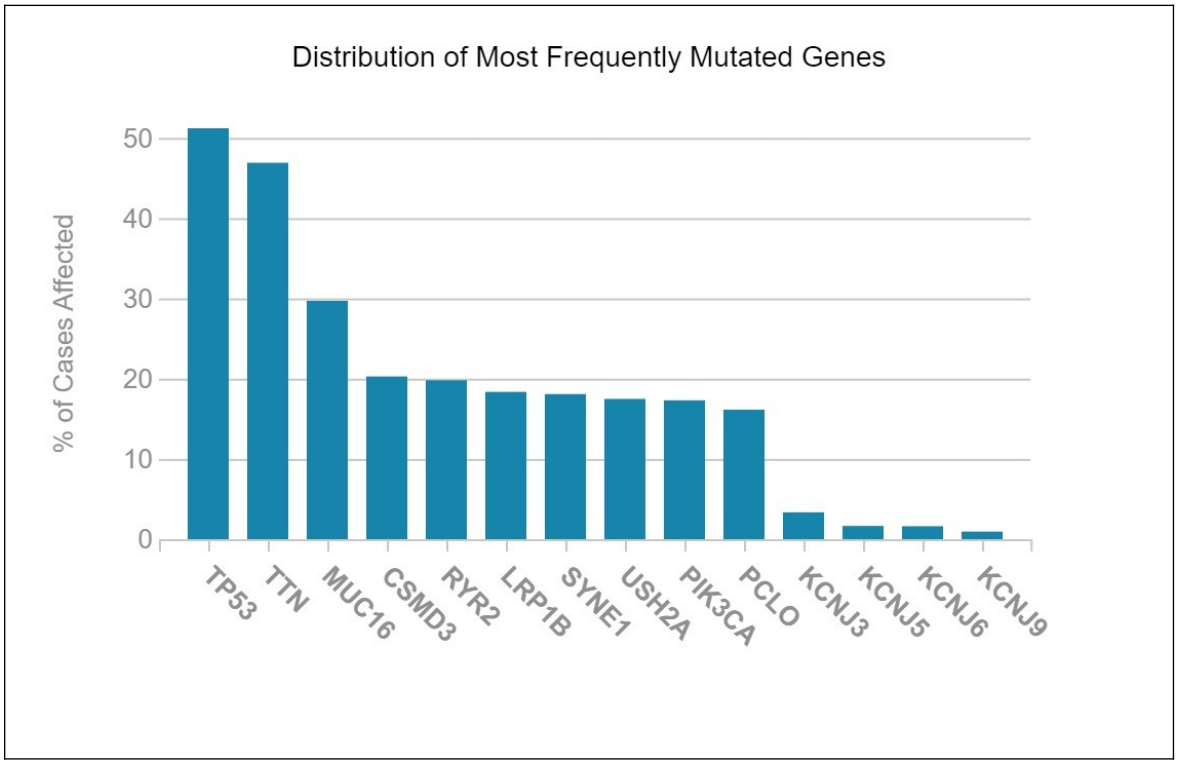

Figure 3: Percentage of somatic mutations in primary tumors of frequently mutated genes in comparison to KCNJ gene family

(Provided from NCI GDC data portal), https://portal.gdc.cancer.gov/exploration?fac From Dec. 2022.

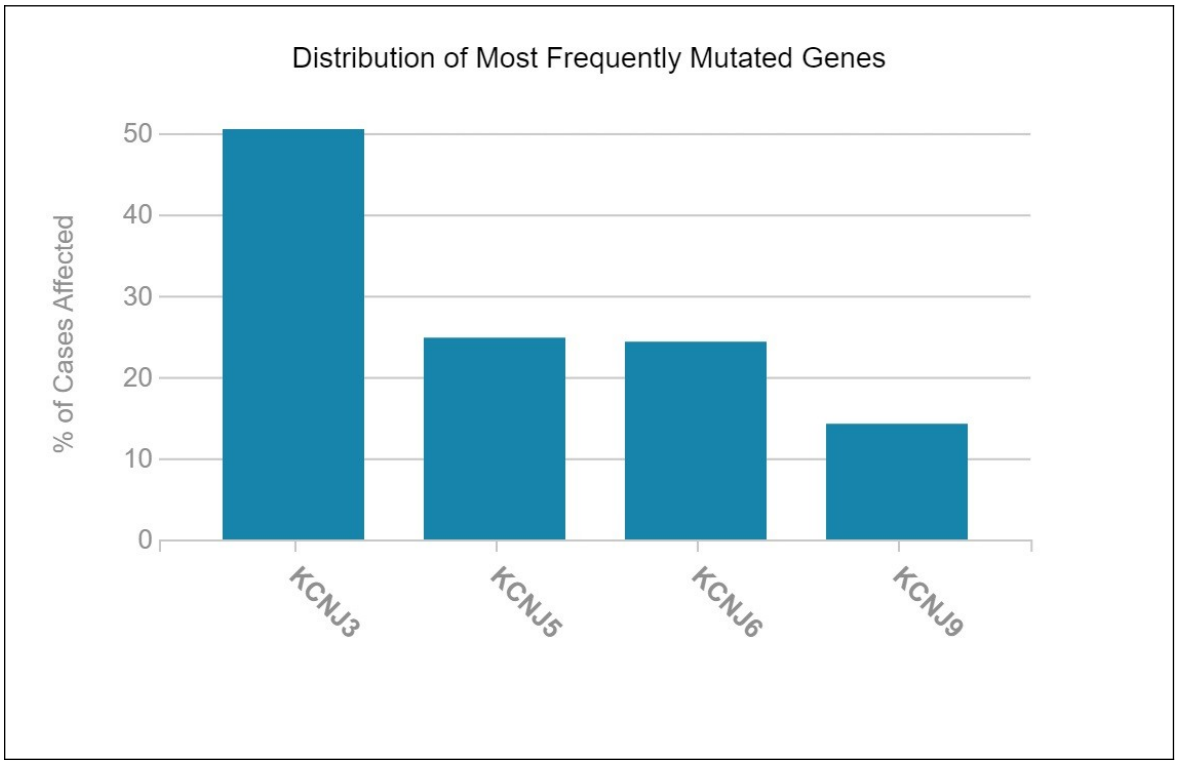

Figure 4: Percentage of somatic mutations in primary tumors: comparison of the KCNJ gene family

(Provided from NCI GDC data portal), https://portal.gdc.cancer.gov/exploration? From Dec. 2022.

Table 1: Data provided by NCI GDC data portal from 26 Projects with about 305 cases affected by 321 mutations of the KCNJ3 gene

(From NCI GDC data portal), https://portal.gdc.cancer.gov/genes From Dec. 2022.

Project	Disease Type	Site	SSM Affected Cases
TCGA-UCEC	Adenomas and Adenocarcinomas, Cystic, Mucinous and Serous Neoplasms, Epithelial Neoplasms	Corpus uteri, Uterus	50 / 512 (9.77%)
TCGA-SKCM	Nevi and Melanomas	Skin	37 / 470 (7.87%)
TCGA-LUAD	Acinar Cell Neoplasms, Adenomas and Adenocarcinomas, Cystic, Mucinous and Serous Neoplasms	Bronchus and lung	42 / 559 (7.51%)
TCGA-LUSC	Squamous Cell Neoplasms	Bronchus and lung	30 / 490 (6.12%)

CMI-ASC	Soft Tissue Tumors and Sarcomas	Bladder, Breast, Bronchus and lung, Heart, mediastinum, and pleura, Lymph nodes, Other and ill-defined digestive organs, Other and ill-defined sites, Other and ill-defined sites within respiratory system and intrathoracic organs, Skin	2 / 36 (5.56%)
TCGA-STAD	Adenomas and Adenocarcinomas, Cystic, Mucinous and Serous Neoplasms	Stomach	23 / 434 (5.30%)
TCGA-COAD	Adenomas and Adenocarcinomas, Complex Epithelial Neoplasms, Cystic, Mucinous and Serous Neoplasms, Epithelial Neoplasms	Colon, Rectosigmoid junction	18 / 427 (4.22%)
HCMI-CMDC	Adenomas and Adenocarcinomas, Complex Epithelial Neoplasms, Complex Mixed and Stromal Neoplasms, Cystic, Mucinous and Serous Neoplasms, Ductal and Lobular Neoplasms, Gliomas, Miscellaneous Bone Tumors, Myomatous Neoplasms, Nevi and Melanomas, Soft Tissue Tumors and Sarcomas	Bones, joints and articular cartilage of other and unspecified sites, Brain, Breast, Bronchus and lung, Colon, Connective, subcutaneous and other soft tissues, Esophagus, Kidney, Liver and intrahepatic bile ducts, Other and unspecified parts of biliary tract, Pancreas, Rectosigmoid junction, Rectum, Skin, Small intestine, Stomach	4 / 110 (3.64%)
CPTAC-3	Adenomas and Adenocarcinomas, Ductal and Lobular Neoplasms, Gliomas, Squamous Cell Neoplasms	Brain, Bronchus and lung, Kidney, Other and ill-defined sites, Pancreas, Uterus	30 / 1,029 (2.92%)
TCGA-HNSC	Squamous Cell Neoplasms	Base of tongue, Bones, joints and articular cartilage of other and unspecified sites, Floor of mouth, Gum, Hypopharynx, Larynx, Lip, Oropharynx, Other and ill-defined sites in lip, oral cavity and pharynx, Other and unspecified parts of mouth, Other and unspecified parts of tongue, Palate, Tonsil	12 / 509 (2.36%)

MMRF-COMMPASS	Plasma Cell Tumors	Hematopoietic and reticuloendothelial systems	21 / 959 (2.19%)
TCGA-DLBC	Mature B-Cell Lymphomas	Bones, joints and articular cartilage of other and unspecified sites, Brain, Breast, Colon, Connective, subcutaneous and other soft tissues, Heart, mediastinum, and pleura, Hematopoietic and reticuloendothelial systems, Lymph nodes, Other and unspecified major salivary glands, Retroperitoneum and peritoneum, small intestine, Stomach, Testis, Thyroid gland	1 / 47 (2.13%)
TCGA-GBM	Gliomas	Brain	5 / 374 (1.34%)
TCGA-BLCA	Adenomas and Adenocarcinomas, Epithelial Neoplasms, Squamous Cell Neoplasms, Transitional Cell Papillomas and Carcinomas	Bladder	5 / 408 (1.23%)
TCGA-ACC	Adenomas and Adenocarcinomas	Adrenal gland	1 / 90 (1.11%)
TCGA-LIHC	Adenomas and Adenocarcinomas	Liver and intrahepatic bile ducts	4 / 369 (1.08%)
CPTAC-2	Adenomas and Adenocarcinomas, Cystic, Mucinous and Serous Neoplasms, Ductal and Lobular Neoplasms, Squamous Cell Neoplasms	Breast, Colon, Other and unspecified female genital organs, Ovary, Rectum, Retroperitoneum and peritoneum	3 / 328 (0.91%)
TCGA-SARC	Fibromatous Neoplasms, Lipomatous Neoplasms, Myomatous Neoplasms, Nerve Sheath Tumors, Soft Tissue Tumors and Sarcomas, Synovial-like Neoplasms	Bones, joints and articular cartilage of limbs, Colon, Connective, subcutaneous and other soft tissues, Corpus uteri, Kidney, Meninges, Other and unspecified male genital organs, Other and unspecified parts of tongue, Ovary, Peripheral nerves and autonomic nervous system, Retroperitoneum and peritoneum, Stomach, Uterus	2 / 235 (0.85%)

TCGA-CESC	Adenomas and Adenocarcinomas, Complex Epithelial Neoplasms, Cystic, Mucinous and Serous Neoplasms, Squamous Cell Neoplasms	Cervix uteri	2 / 287 (0.70%)
TCGA-READ	Adenomas and Adenocarcinomas, Cystic, Mucinous and Serous Neoplasms	Colon, Connective, subcutaneous and other soft tissues, Rectosigmoid junction, Rectum	1 / 155 (0.65%)
TCGA-KIRC	Adenomas and Adenocarcinomas	Kidney	2 / 330 (0.61%)
TCGA-ESCA	Adenomas and Adenocarcinomas, Cystic, Mucinous and Serous Neoplasms, Squamous Cell Neoplasms	Esophagus, Stomach	1 / 184 (0.54%)
TCGA-BRCA	Adenomas and Adenocarcinomas, Adnexal and Skin Appendage Neoplasms, Basal Cell Neoplasms, Complex Epithelial Neoplasms, Cystic, Mucinous and Serous Neoplasms, Ductal and Lobular Neoplasms, Epithelial Neoplasms, Fibroepithelial Neoplasms, Squamous Cell Neoplasms	Breast	5 / 965 (0.52%)
TCGA-OV	Cystic, Mucinous and Serous Neoplasms	Ovary	2 / 418 (0.48%)
TCGA-KIRP	Adenomas and Adenocarcinomas	Kidney	1 / 277 (0.36%)
TCGA-LGG	Gliomas	Brain	1 / 510 (0.20%)

SSM: Simple somatic mutation

2 Materials and Methods

2.1 Solutions and reagents:

NDE: 96 mmol/L of NaCl, 2 mmol/L of KCl, 1 mmol/L of $MgCl_2$, 1.8 mmol/L of $CaCl_2$, 2.5 mmol/L of pyruvate, 0.1% antibiotics (G-1397; ·1000 stock from Sigma-Aldrich) and 5 mmol/L Hepes buffered with NaOH to pH 7.4; **ND96**: 96 mmol/L of NaCl, 2 mmol/L of KCl, 1 mmol/L of $MgCl_2$, 1 mmol/L of $CaCl_2$, 5 mmol/L of Hepes buffered with NaOH to pH 7.4; **HK**: 96 mmol/L of KCl, 2 mmol/L of NaCl, 1 mmol/L of $MgCl_2$, 1

mmol/L of $CaCl_2$, 5 mmol/L of Hepes buffered with NaOH to pH 7.4; **HK0**: 0 mmol/L of KCl, 98 mmol/L of NaCl, 1 mmol/L $MgCl_2$, 1 mmol/L $CaCl_2$, 5 mmol/L Hepes buffered with NaOH to pH 7.4; **HK2**: 2 mmol/L of KCl, 96 mmol/L of NaCl, 1 mmol/L $MgCl_2$, 1 mmol/L $CaCl_2$, 5 mmol/L Hepes buffered with NaOH to pH 7.4; **HK8**: 8 mmol/L of KCl, 90 mmol/L of NaCl, 1 mmol/L $MgCl_2$, 1 mmol/L $CaCl_2$, 5 mmol/L Hepes buffered with NaOH to pH 7.4; **HK24**: 24 mmol/L of KCl, 74 mmol/L of NaCl, 1 mmol/L $MgCl_2$, 1 mmol/L $CaCl_2$, 5 mmol/L Hepes buffered with NaOH to pH 7.4; **HK72**: 72 mmol/L of KCl, 26 mmol/L of NaCl, 1 mmol/L $MgCl_2$, 1 mmol/L $CaCl_2$, 5 mmol/L Hepes buffered with NaOH to pH 7.4. **GIRK1-Antibody**: Anti-Kir3.1 (APC-005; Alomone Labs, Ltd). **GAPDH-Antibody**: Proteintech Cat. No.: 60004. **KHA2** antisense oligonucleotide synthesized by Mycrosynth ("desalted" grade; Mycrosynth AG). Unless otherwise specified, any additional reagents included were of the same caliber.

2.2 Genetic construction and verification:

All the genetic engineering has been prior conducted and stored in a freezer at -80C°. To briefly describe, (Jing, Chikvashvili et al. 1999) summarizes the production of plasmids for the G-protein $G_\beta 2$ and $G_\gamma 1$ subunits. (Wagner, Stadelmeyer et al. 2010) and (Treiber, Rosker et al. 2013) detailed the synthesis of plasmids containing the human GIRK4 and m2R genes, as well as the human GIRK1 that has been N-terminally tagged with eGFP ($GIRK1^{eGFP}$). According to (Treiber, Rosker et al. 2013) instructions, point mutation construction and mRNA synthesis were carried out. Sanger sequencing was implemented to confirm the sequence of each produced genome research model (Microsite AG; Austria; Vienna).

2.3 Xenopus laevis Oocytes expression and Two Electrode Voltage clamp (TEVC):

Procedure and management of Xenopus oocytes adhered to the instructions by (Hedin, Lim et al. 1996). Oocytes have been defolliculated by using 2 mg/ml collagenase for 2–3 h, about 24 hours after their isolation oocytes were inoculated with the appropriate quantity of mRNA and KHA2 antisense oligonucleotide to block down endogenous subunit (Hedin, Lim et al. 1996). Quantities of antisense oligonucleotides and mRNA, injected into each oocyte, were as follows: KHA2: 25ng, $GIRK1^{eGFP}$ (WT and mutants) 1ng, GIRK4: 1ng and m_2R: 1.5ng. (Unless otherwise specified, KHA2 was always injected in the quantity specified.). Before conducting tests, injected oocytes were maintained in NDE at 19°C for 3-5 days. Oocytes were put in an observing compartment where they could be superfused with ND96, HK, and HK with 10^{-5} mol/L acetylcholine at 21°C for the TEVC experiment Agarose cushioned electrodes (Schreibmayer, Lester et al. 1994) and the Geneclamp 500

amplifier were used to record currents (Axon Instruments, Foster City, CA, USA). Experimental medium was alternated from ND96→HK→HK+ acetylcholine succeeding washout with HK + acetylcholine→ND96, while maintaining the membrane potential at -80 mV (Wagner, Stadelmeyer et al. 2010). Using the Digidata 1550B interface from Axon Instruments in Foster City, California, the United States, current traces were low pass filtered at 10 Hz and digitalized at a sampling rate of 4ms while connected to an Intel-Chipset based computer operating PClamp 11.0 software (Axon Instruments, Foster City, CA, USA). The experimental medium was changed to HK24 + acetylcholine for oocytes that produced currents greater than 10 mA in HK + acetylcholine and empirical modification was used to adjust the current amplitude (multiplication factor for IHK24 adjustment was 1.612 ±0.079 SEM, calculated from 8 experimental days). The P_{Na+}/P_{K+} ratio has been calculated likewise to (Shalomov, Handklo-Jamal et al. 2022), namely, the Goldman-Hodgkin-Katz equation, as shown in the equation (1) below, was used to estimate the permeability ratio of sodium and potassium (P_{Na+}/P_{K+}).

(1)

$$E_{rev} = \frac{R.T}{z.F} log\left(\frac{pK^+[K^+]_o + pNa^+[Na^+]_o}{pK^+[K^+]_i + pNa^+[Na^+]_i}\right)$$

F is the Faraday constant, T is the absolute temperature, R is the gas constant, and z is the valence (i.e., 1 for Na^+ and K^+) in equation (1), $[K^+]_o$ represents the extracellular K^+ concentration, $[K^+]_i$ represents the intracellular K^+ concentration, $[Na^+]_o$ represents the extracellular Na^+ concentration, $[Na^+]_i$ represents the intracellular Na^+ concentration.

In order to permanently activate GIRK, G_β (2.5 ng/oocyte) and G_γ (0.5 ng/oocyte) subunit mRNA were administered. To achieve optimal ion currents in HK72, ranging from 1 to 4 mA, when necessary (in contrast to the experimental framework used for the expression/function analyses), it was necessary to alter the quantity of GIRK1 and GIRK4. This allowed for an appropriate measure of the reversal potential. The following mRNA injection rates ($GIRK1^{eGFP}$/GIRK4 mRNA in ng/oocyte) were used to generate the various constructs: **GIRK4** (homooligomer): 5-10 ng; **WT/GIRK4**: 0.65 ng /0.65 ng; **S132Y/GIRK4**: 1.25 ng /1.25 ng; **L135I/GIRK4**: 0.1- 0.5 ng /0.1-0.5 ng; **F136L/GIRK4**: 0.5-5 ng /0.5-5 ng; **E140M/GIRK4**: 2.5 ng /2.5 ng; **A142T/GIRK4**: 0.1 ng /0.1 ng; **G145A/GIRK4**: 0.5-2.5 ng /0.5-2.5 ng; **R149Q/GIRK4**: 1.25-12.5 ng /1.25-12.5 ng; **I151N/*G*IRK4**: 12.5 ng /12.5 ng; **M184I/GIRK4**: 0.2-0.5 ng /0.2-0.5 ng and **Q186R/GIRK4**: 1 ng /1 ng. The oocytes underwent TEVC after 3-5 days of incubation. The membrane potential was maintained at -80 mV, and once the resting current had stabilized, the perfusion was altered and the $[K^+]$ concentration was raised incrementally from ND96→ 2HK→ 8HK→ 24HK→ 72HK. Using a Minidigi 1A digitizer, the whole

experiment was measured continuously at a sample rate of 4 ms (Axon Instruments, Foster City, CA, USA). A voltage ramp with a length of 2 seconds from -120 mV to +50 mV was administered once the holding current had stabilized at a certain perfusion medium and both current and voltage were monitored individually (sample rate 2 ms; Digidata 1550B; Axon Instruments, Foster City, CA, USA). Afterwards, the perfusion media were then switched in the opposite order, however 2 mmol/L $Ba2^{+}$ had been present in the media to inhibit currents through GIRK channels (see Figure 13 for experimental protocol). When measuring the ramp current in a particular medium, the background ramp current recorded under 2 mmol/L Ba^{2+} was subtracted from the ramp current measured without Ba^{2+} and displayed as a function of the observed membrane potential (see Figure 14). The reversal potential was also measured (see Figure 15). The Goldman equation was solved for the permeability ratio P_{Na+}/P_{K+} for a particular pair of reversal potentials (E_{rev1} and E_{rev2}), measured at two distinct extracellular K^{+} and Na^{+} concentrations $[K^{+}]_1^0$, $[K^{+}]_2^0$, $[Na^{+}]_1^0$ and $[Na^{+}]_2^0$, respectively; Equations (2-4) as shown below:

(2)

$$\frac{PNa^{+}}{PK^{+}} = \left(\frac{[\mathrm{K^{+}}]_1^0 - \mathrm{A} \cdot [\mathrm{K^{+}}]_2^0}{\mathrm{A} \cdot [\mathrm{Na^{+}}]_2^0 - [\mathrm{Na^{+}}]_1^0} \right)$$

(3)

$$A = \frac{e^{\frac{E_{rev1}}{v_0}}}{e^{\frac{E_{rev2}}{v_0}}}$$

(4)

$$v_0 = \frac{R.T}{z.F}$$

P_{Na+}/P_{K+} was then calculated using E_{rev1} and E_{rev2}, as well as the predefined concentrations $[K^{+}]_1^0$, $[K^{+}]_2^0$, $[Na^{+}]_1^0$ and $[Na^{+}]_2^0$. The maximum quantity of mRNA encoding GIRK1 and GIRK4 (i.e., 12.5 ng/oocyte per mRNA species) combined with m2R (1.5 ng/oocyte) was administered for constructions (i.e., E139K, R149P, G158S, G178D, and S185Y) that did not give currents large enough to permit the precise calculation of the P_{Na+}/P_{K+} ratio. These oocytes underwent a straightforward, entirely qualitative procedure: first, at -80 mV, the medium was switched from ND96→HK→HK+acetylcholine followed by a washout from HK→ND96 in order to confirm appropriate functional expression of the GIRKs. Second, HK0→HK0+acetylcholine was superfused into the oocytes. A noticeable increase in the retaining current by acetylcholine should have been visible in HK0 in the scenario of a complete loss of K^{+} selectivity and considerable Na^{+} penetration

through open GIRK channels. However, none of the examined structures showed this to be the case (data not shown).

2.4 Confocal laser scan microscopy (cLSM):

The cLSM scan of the oocytes has been carried out as originally described by (Wagner, Stadelmeyer et al. 2010). To sum things up, the very same oocytes underwent cLSM immediately following TEVC to measure the quantity of eGFP tagged GIRK1 subunit at or near the oocyte's plasma membrane. A Leica inverting microscope with a laser scanning attachment was used to scan oocytes in NDE solution (DMIRE2 and TCS SL2; Leica Microsystems, Heidelberg, Germany). Using the 20x (NA: 0.50) water immersed objective, confocal slices from a location just underneath the oocyte's equator were produced with a 12-bit resolution (512x512 pixels), from 2 to 4 oocytes were taken in one image as shown in (Figure 5). The fluorophore detection and excitation filters were adjusted to: eGFP: excitation (488 nm); excitation beam splitter TD 488/543/633; emission (500–530 nm). For a certain testing day, the instrument settings—namely, the pinhole size, laser intensity, and PMTs' gain and offset—were held constant and for every experimental day the eGFP fluorescence was normalized to the group solely expressing hGIRK1a^{eGFP}/hGIRK4^{WT} heterooligomeric GIRK channels (Wagner, Stadelmeyer et al. 2010). The ImageJ program (version 1.42 by Wayne Rasband, NIH, Bethesda, MD) was used for quantitative analysis of confocal images.

2.5 Statistics and the normalization of data:

All measured ΔF (difference in fluorescence intensity between the membrane and the background) or I_{total} (Total electric current = I_{HK} + I_{ACh}) values were normalized to readings of the WT (wild type) GIRK1^{eGFP}/GIRK4 heterooligomeric channel of a specific experimental day and batch of oocytes in order to remove scatter caused by batch-to-batch fluctuation of protein expression among oocytes batches. MATLAB® R2022a and the free software R 4.2.1 were used to statistically analyze the data given in (Table 2) and Table 4, Table 5, Table 6 (and visually in Figure 6, Figure 9, and Figure 16). The bootstrap-t approach about 2000 repetitions was used to establish a consistent inferential statistical assessment after evaluating the data's approximative normal distribution i.e., z-value of skewness and kurtosis, Q-Q plot, and p value of Shapiro-Wilk test. To compare two independent means, one-way ANOVA and multiple comparisons to a control group (Dunnett T3 technique), the R functions yuenbt(), t1waybt(), and linconbt() had been used respectively (30). A one-way ANOVA was applied to examine all other experimental parameters for statistically significant variations. Kruskal Wallis One Way Analysis of

Variance was performed if the data had not been normally distributed (SPSS package in Sigmaplot 14.5; Systat Software).

3 Results

A search on the GDC data portal revealed 305 cancer cases out of 13,714 cases of primary malignant tumors of any origin that exerted 321 somatic mutations of the KCNJ3 subunit gene. Lung, cutaneous, and uterine malignancies had the highest rates of somatic mutations in KCNJ3 (data from Dez. 2022). Further consideration was not given to mutations that had occurred in the 3' or 5' untranslated regions or equivalent mutations in the DNA that did not impact the amino acid sequence. Similar procedures were done for mutations that resulted in frameshifts, which produced shortened and consequently most likely non-functional proteins. Figure 17 shows the locations of all missense mutations found in the 501 amino acid primary structure of GIRK1. We focused exclusively on a location near the primary structure responsible for ion selectivity of GIRK channels, namely around the P- helix, the hallmark of ion (Nishida, Cadene et al. 2007). It has already been demonstrated that somatic mutations of amino acids inside or close to the analogous area of GIRK4 subunit, render GIRK ion channels unselective for K^+ over Na^+ and are responsible for the development of benign adrenal cortical adenomas (Mulatero, Monticone et al. 2013). The implication that multiple somatic mutations gathered around F137 served as further motive to investigate this area. The GIRK1 subunits that contain mutation F137S (which has only ever been synthesized in the research facility, but so far never was observed in real organisms) are capable of generating functional homooligomeric ion channels (Chan, Sui et al. 1996). Considering S185 has been reported as being crucial for Protein kinase-C modulation of GIRK1 (Mao, Wang et al. 2004) and we recognized somatic mutations there too and nearby, mutations in the minor section at the cytosolic end of TM2 were also investigated. For a summary of the area and the researched amino acids see Figure 7. Using the GIRK1 subunit with the eGFP marker and quantitative confocal laser scan microscopy cLSM, it was possible to examine expression levels of GIRK1 protein and the various mutants' proteins in Xenopus oocytes. Figure 5 shows typical selected confocal images (transmission and fluorescence) of oocytes injected with different GIRK1 variants. Figure 6 displays the statistical analysis of protein expression levels in the presence and absence of coexpression of the GIRK4 subunit (see Table 4 for numerical data and statistical parameters). Overall fluorescence levels of GIRK1 subunits, that have been simultaneously injected with GIRK4, were typically higher, showcasing that expression of protein close to and/or at the plasma membrane is

more intense whenever GIRK1 and GIRK4 were coexpressed, compared to GIRK1 expression alone. Albeit the mutants I151N and G158S displayed the poorest protein expression of any of the mutants, the expression levels observed were, statistically, significant.

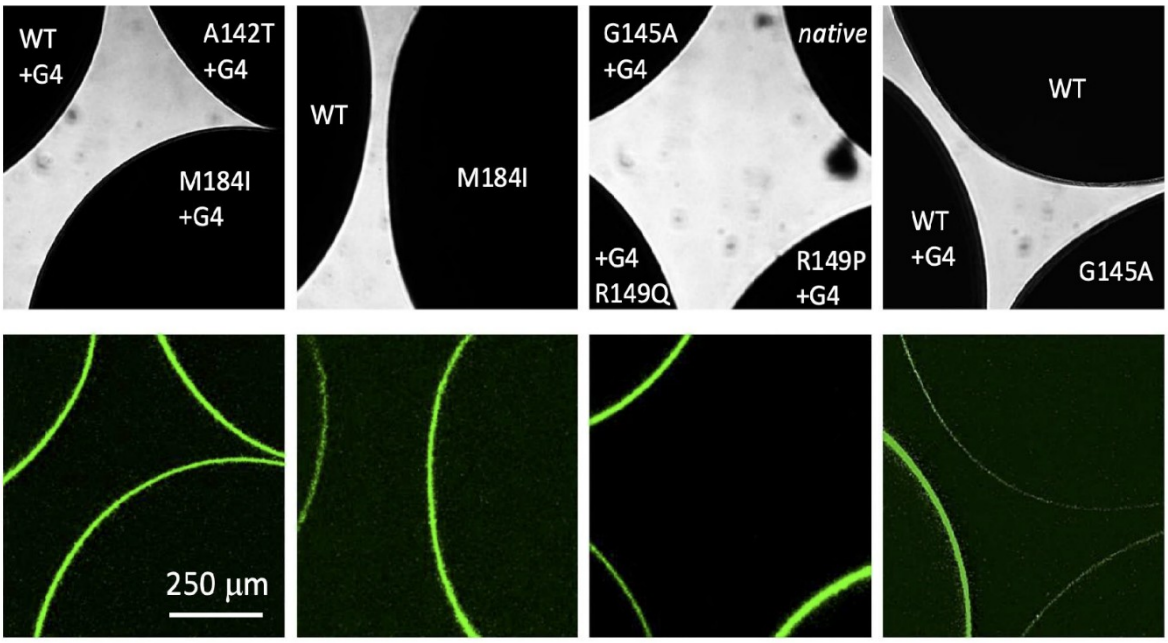

Figure 5: Quantitative expression of GIRK1 subunit mutations. Original micrographs of oocytes expressing different GIRK1 constructs with and without GIRK4 coexpressed. Upper row: Transmission. Lower row: Fluorescence.

From (Pelzmann, Hatab et al. 2022).

Using the Two Electrode Voltage Clamp procedure, the viability of the various mutants as GIRK ion channels, both with and without GIRK4 coexpression, was evaluated. See Figure 8 for selected, typical original current traces. Instead of using the current triggered by acetylcholine as a measure of a mutation's functioning, we opted total current, which includes both baseline current and as well as the current induced by activated, coexpressed muscarinic type 2 receptors (m2Rs). In the majority of gene mutations, I_{ACh}/I_{total} ratios roughly equivalent to GIRK1^{WT}/GIRK4 were observed. I_{ACh}/I_{total} ratios were statistically significantly distinct for I151N and S185Y, with I151N showing a statistically significant rise, and S185Y showing a statistically significant decrease. Further research is required to discover if I151N and S185Y affect the channels' ability to be activated by G-protein β/γ (See Figure 18 and Table 5 for exact values and statistics of I_{ACh}/I_{total} ratios).

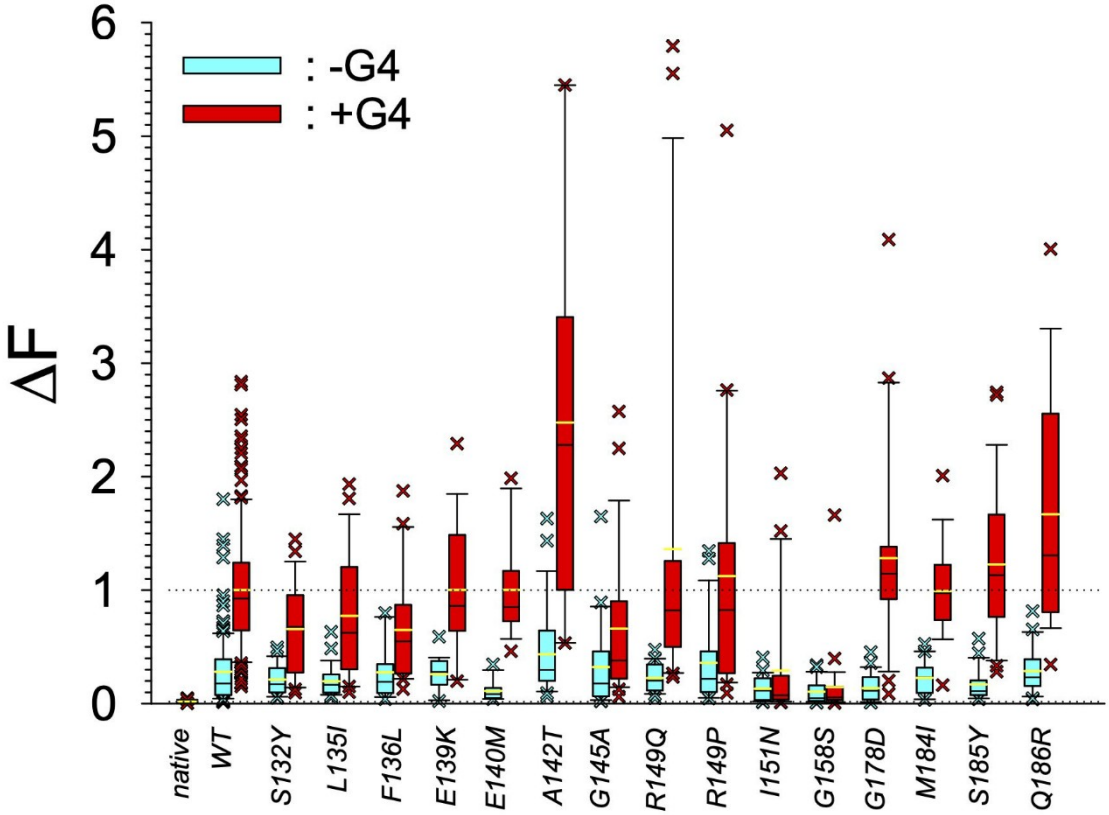

Figure 6: Quantitative expression of GIRK1 subunit mutations.

Expression levels of different GIRK1eGFP subunit mutations, relative to WT. Blue boxes: GIRK1 mRNA injected alone. Red boxes: GIRK1 was co-injected with GIRK4 mRNA. Box plots comprise 25% and 75% percentiles. Median (solid black line within box) and average value (yellow line) indicated within box. Whiskers denote 10% and 90% percentiles. Oocytes having values above 90% and below 10% percentiles are shown as cross. 14 – 142 oocytes per experimental group. From (Pelzmann, Hatab et al. 2022).

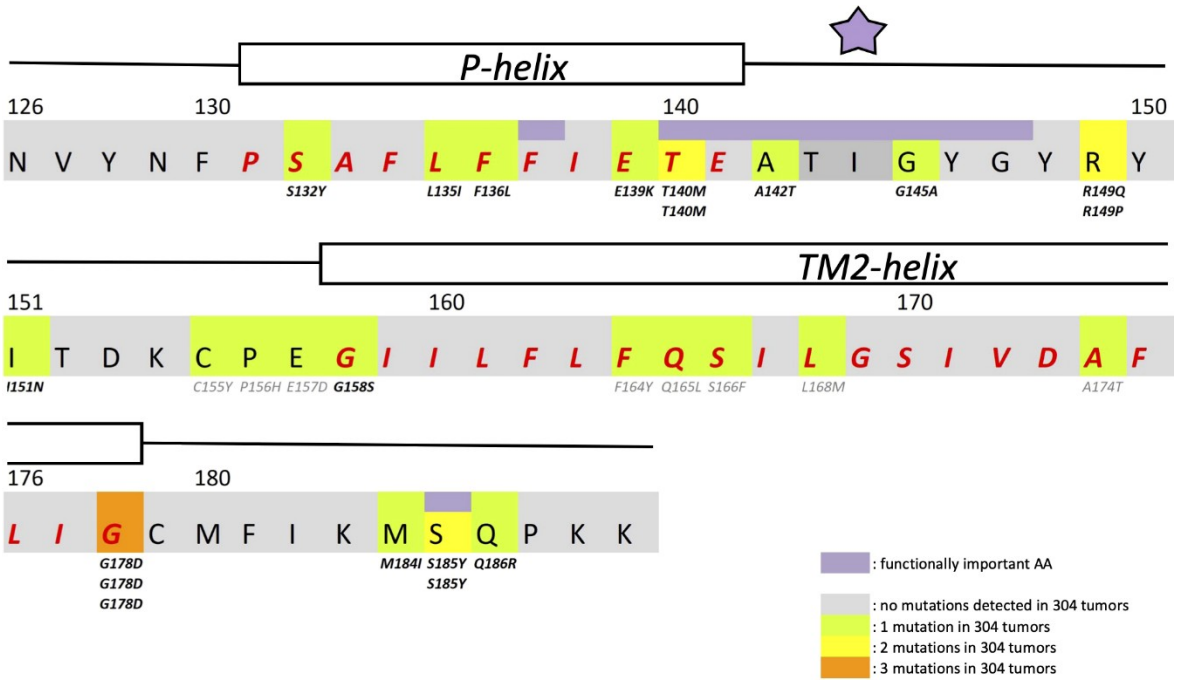

Figure 7: Somatic cancer mutations in the primary structure of the human GIRK1 subunit, adjacent to P-helix.

Partial primary structure of the human GIRK1 subunit. Amino acid numbering according to entire full length variant 1a. Regions comprising the pore helix and the transmembrane helix 2 are indicated and the corresponding amino acids emphasized in red. Amino acids of outstanding interest are highlighted in purple (F137, ion selectivity signature (indicated by a purple asterisk) and S185). Somatic mutations detected are highlighted in green (1 mutation found), yellow (2 mutations found) and orange (3 mutations found). Multiple appearance of a mutation underneath an amino acid residue indicates multiple occurrences in different tumors of the sample cohort. From: (Pelzmann, Hatab et al. 2022).

The majority of mutants are unable to produce substantial ion currents when injected alone, as shown in Figure 9 (see also Table 6). As shown in Figure 10, two mutations, A142T and M184I, look noteworthy because they have higher fluorescence and total current compared to WT injected alone. It is well documented that WT GIRK1 subunits cannot assemble into functional homooligomeric ion channels (Hedin, Lim et al. 1996). As a result, the negligible total current, which is around 5% of the current produced by WT plus GIRK4, detected in WT alone is the result of insufficient antisense oligonucleotide suppression of the endogenous GIRK5 subunit in the frog oocyte.

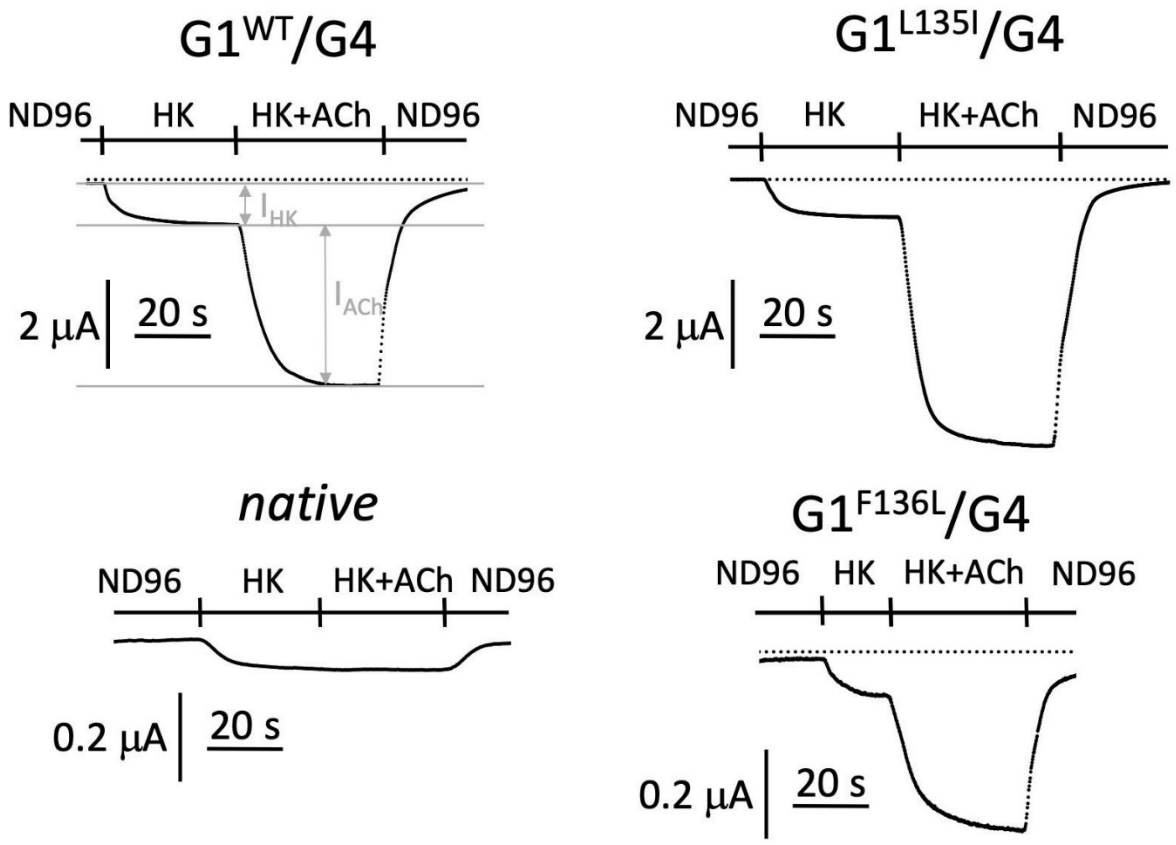

Figure 8: Current amplitudes produced by the different GIRK1 mutations.
Representative original TEVC current recordings, produced by different GIRK1 subunits, at a holding potential of -80 mV. Super-fusion medium was exchanged as indicated above the traces. From: (Pelzmann, Hatab et al. 2022).

Therefore, the increased amount of current for A142T and M184I injected alone may indicate a gain in the capacity to assemble functional homotetrameric ion channels. Hence, we examined the homooligomeric GIRK channel formation potential of A142T and M184I in more detail: Total current values and fluorescence were compared to WT after injecting increasing quantities of GIRK1 mRNA alongside and without the antisense oligonucleotide (Figure 11). As would be anticipated, the quantity of injected mRNA resulted in a slight increase in expression in WT. As seen by the decreased fluorescence levels after oligonucleotide coinjection, the endogenous GIRK5 subunit enhances expression and/or localization at or near the plasma membrane. The coinjection of such antisense oligonucleotide noticeably and statistically lowered the total current amplitudes, while the dose of mRNA injected had no significant impact on total current amplitudes. This is precisely what should be expected when the endogenous GIRK5 subunit is the rate limiting step for functional ion channel formation and when GIRK1 homooligomeric ion channel formation is not feasible. Therefore, heterooligomeric ion channels encompassing

endogenous GIRK5 that became left behind during antisense oligonucleotide knockdown are accountable for generating the weak but detectable ion current. Both A142T and M184I displayed a similar pattern of behavior, demonstrating that these mutants lack the ability to form homomers and need GIRK4 for the construction of functional ion channels, much like WT. When compared to WT, current values for A142T were regularly higher than it was for fluorescence at all the mRNA quantities examined, suggesting that heterooligomeric ion channel complexes comprising this mutation may have a higher open probability, compared to their WT counterparts, but the ability to form homomers is absent.

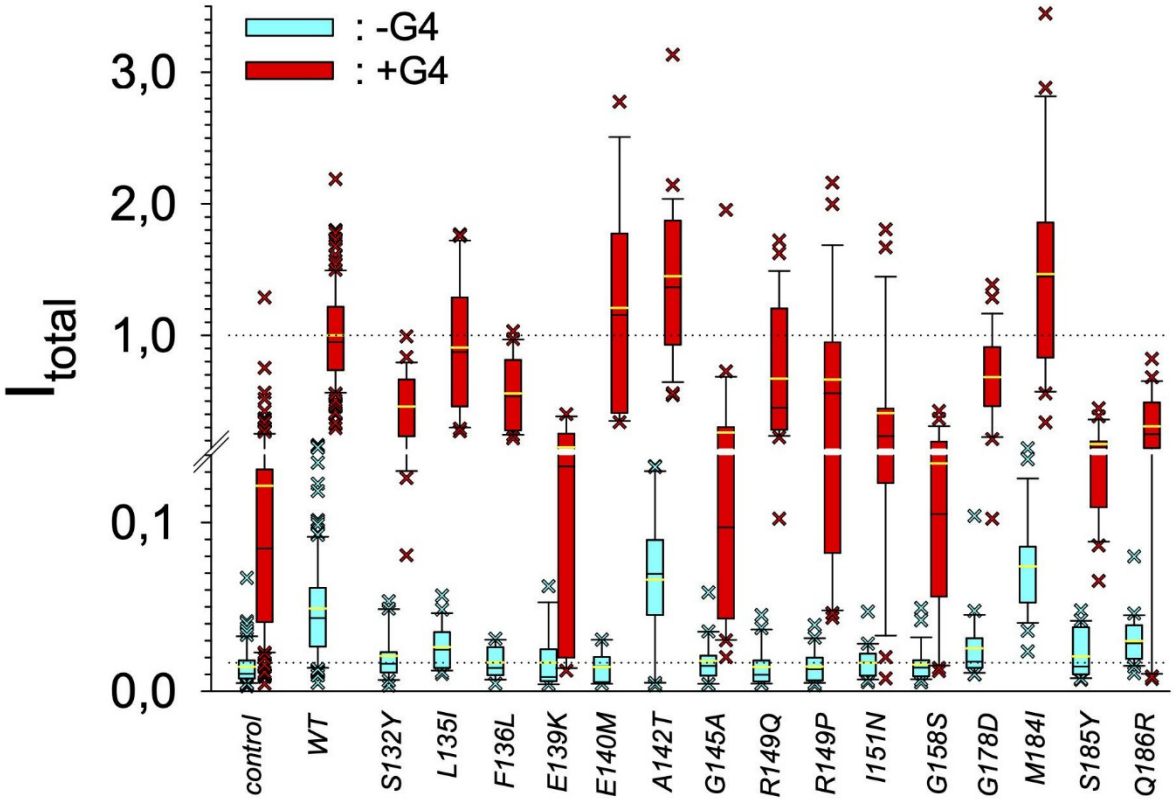

Figure 9: Total current amplitudes

Total current amplitudes generated by various GIRK1^{eGFP} subunit mutations in comparison to WT. GIRK1 mRNA was only injected in the blue boxes. GIRK1 and GIRK4 mRNA were co-injected, as indicated by the red boxes. 25% and 75% percentiles are shown in box plots. Mean values is denoted by the yellow line inside the box, while the median is represented by a solid black line. Whiskers indicate percentiles of 10% and 90%. Oocytes with values above and below the 90% and 10% percentiles are marked individually by a cross. Each experimental group comprises 14 to 145 oocytes. From: (Pelzmann, Hatab et al. 2022).

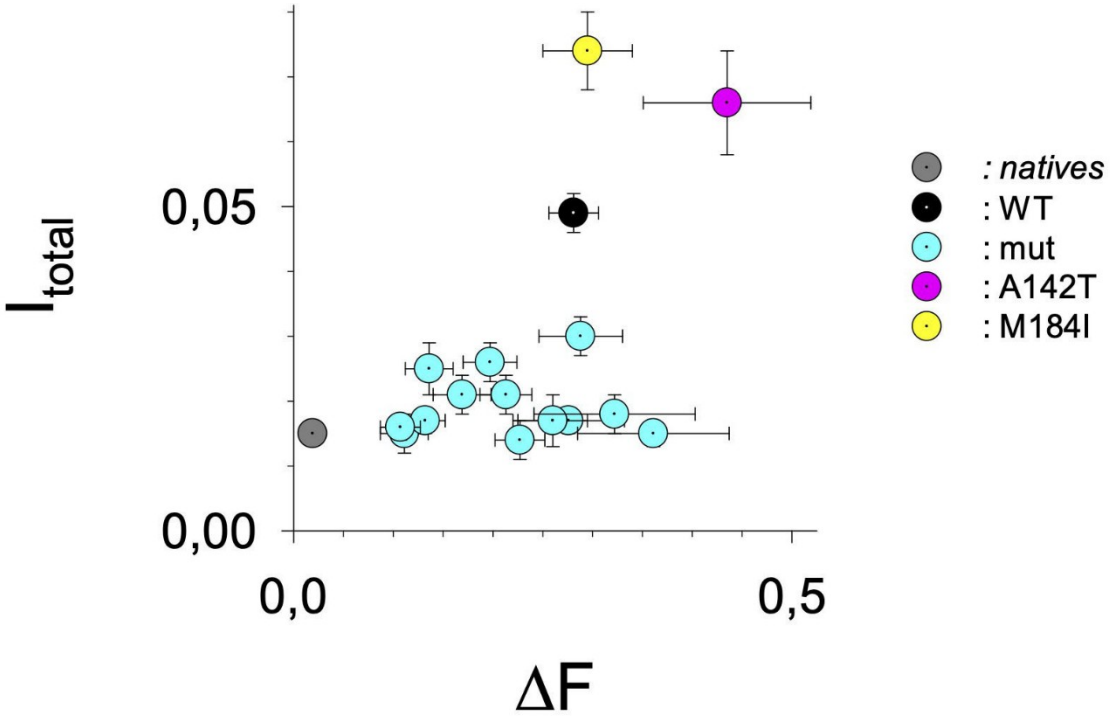

Figure 10: Various GIRK1 mutations injected alone, resulting in different current amplitudes vs expression levels.

Total mean values of the several experimental groups for each experimental day, without the coexpression of the GIRK4 subunit. Within the same testing day and sample of oocytes, I_{total} and ΔF are both normalized to the amounts generated by $GIRK1^{WT}$/GIRK4. Native oocytes are gray, $GIRK1^{WT}$ in black, $GIRK1^{A142T}$ in purple, $GIRK1^{M184I}$ in yellow, and all other GIRK1 subunit mutations studied are cyan. Whiskers stand for SEMs.

From: (Pelzmann, Hatab et al. 2022).

We conclude that none of the mutations evaluated can produce functional homomeric ion channels, and the little amounts of currents that were observed were the result of insufficient antisense oligonucleotide silencing of the endogenous GIRK5 subunit. The majority of the variants have the capacity to generate functional heteromeric GIRK1/GIRK4 ion channels (Figure 9). Currents in the magnitude of WT+GIRK4 are produced by S132Y, L135I, F136L, E140M, A142T, R149Q, R149P, G178D, and M184I (Figure 9; see Table 6 for numerical data and statistics).

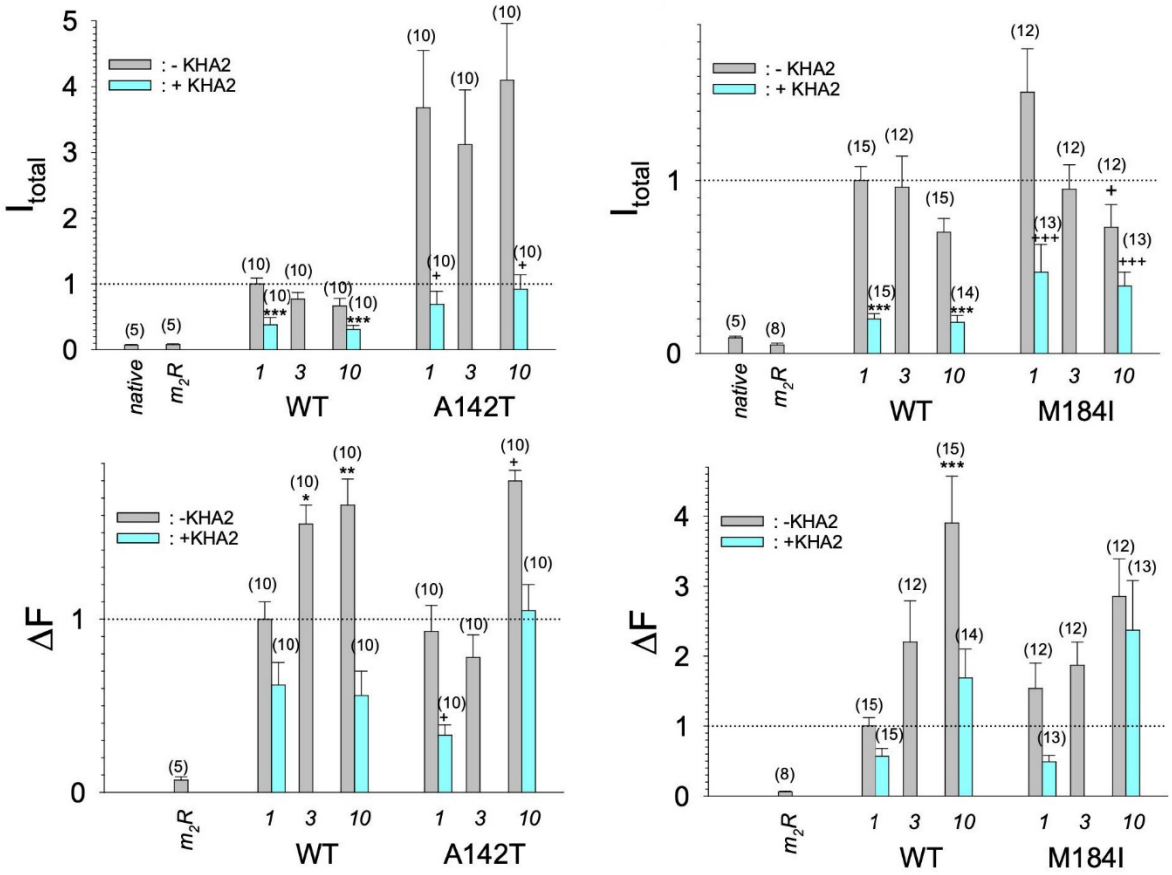

Figure 11: Effect of increasing amounts of GIRK1 mRNA injected on total current amplitudes and expression levels.

Upon injection of various quantities of mRNA encoding for GIRK1^{WT}, GIRK1^{A142T} or GIRK1^{M184I} in ng at bottom of graphs, the total current and ΔF values are shown. The mean values of the specified experimental group are shown as bars. Grey indicates the absence of KHA2 antisense oligonucleotide, while cyan indicates co-injection of mRNA and KHA2 antisense oligonucleotide. Oocytes quantity is indicated in parentheses above the bars. Whiskers indicate SEM. *, **, ***: at the p>0.05, 0.01, and 0.001 values, the mean value varies statistically significantly from the GIRK1^{WT} (without co-injecting KHA2 antisense oligonucleotide). +, ++, +++: At the p>0.05, 0.001, and 0.001 values, the mean value varies statistically significantly from the GIRK1^{A142T} and GIRK1^{M184I} (in absence of KHA2 antisense oligonucleotide). From: (Pelzmann, Hatab et al. 2022).

When GIRK4 is coexpressed, the majority of mutants yield expression levels comparable to WT+GIRK4 and equivalent or lower range of total current Figure 12.

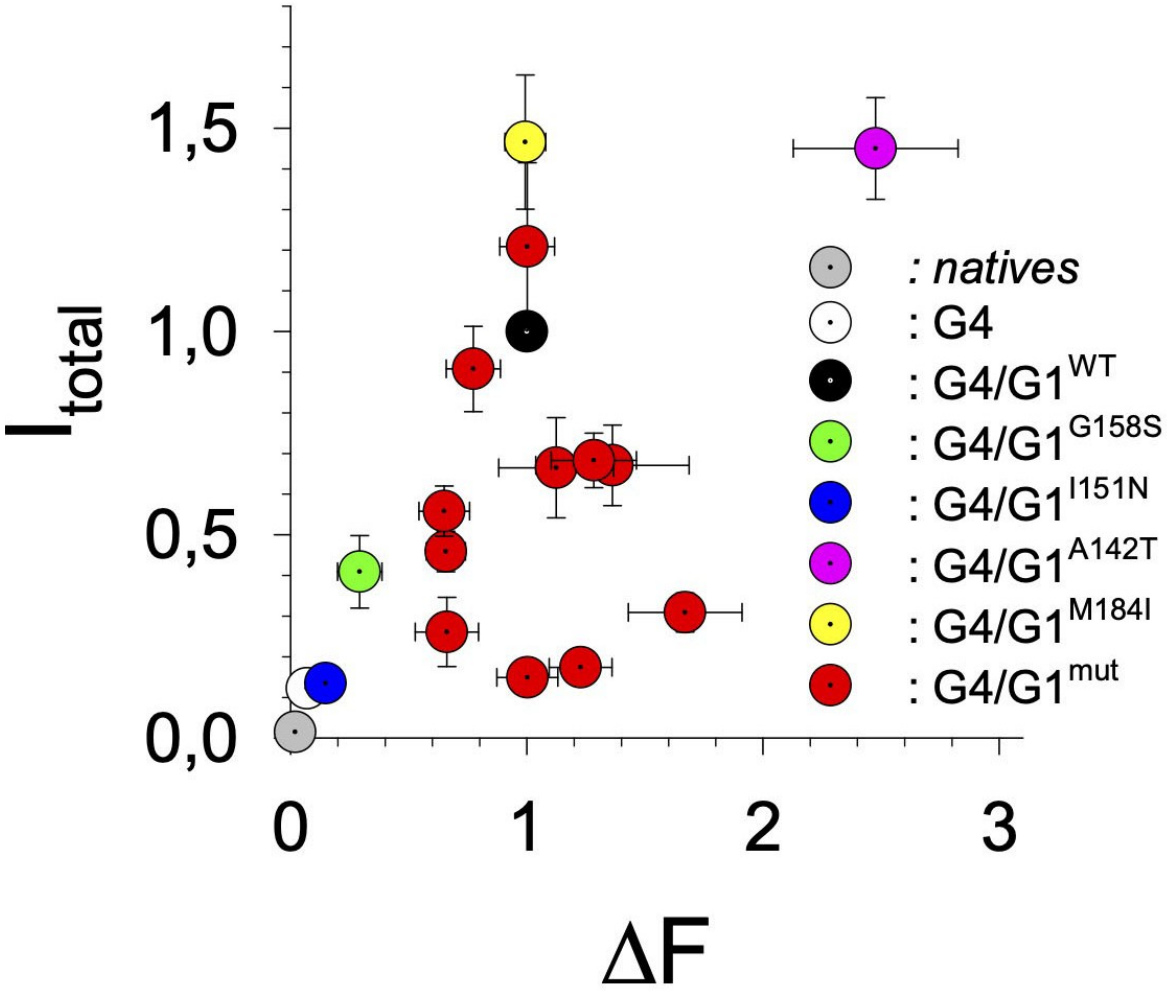

Figure 12: Relation between expression levels and total current amplitudes exerted by the different GIRK1 mutations expressed as GIRK1/GIRK4 heterotetrameric ion channels.

Mean values of the GIRK1/GIRK4 heterotetramer-produced experimental groups' ΔF in proportion to I total for each experimental day. For the same experimental day and batch of oocytes, I total and ΔF were also normalized to the amounts obtained by $GIRK1^{WT}$/GIRK4. Grey represents native oocytes, white: GIRK4 homotetrameric ion channels, black: $GIRK1^{WT}$/GIRK4, purple: $GIRK1^{A142T}$/GIRK4, yellow: $GIRK1^{M184I}$/GIRK4, green: $GIRK1^{G158S}$/GIRK4, blue: $GIRK1^{I151N}$/GIRK4, and red represents all other GIRK1 subunit mutations/GIRK4 tested. Whiskers stand for SEM. From: (Pelzmann, Hatab et al. 2022).

Particularly noteworthy are the I151N and G158S, which produce observable currents in spite of extremely low expression levels, implying an unexpectedly large level of function for each expressed protein.

At various extracellular K^+ concentrations, the reversal potentials of currents across GIRK1/GIRK4 heterotetramers were measured and the ratio of permeability for K^+ and Na^+ (P_{Na+}/P_{K+}) was assessed. (See Figure 13 for a selected typical original current trace resulting from the experimental paradigm applied for the assessment of the P_{Na+}/P_{K+} ratio and Figure 14 & Figure 15 for the measurement and analysis of reversal potentials). For WT and the mutants S132Y, L135I, F136L, E140M, A142T, G145A, R149Q, I151N,

M184I, and Q186R, precise measurement of P_{Na+}/P_{K+} was achievable (see Figure 16). When compared to WT heterooligomeric ion channel, it is obvious that G145A has significantly enhanced P_{Na+}/P_{K+} For GIRK4 homooligomeric ion channels and the other mutations under study, the P_{Na+}/P_{K+} ratio remained unaltered (For specific data and statistics, see Table 2).

Table 2: Statistics of P_{Na+}/P_{K+} ratios.

	P_{Na+}/P_{K+} mean	SEM	N	p-value (WT vs. mutant)
WT	0,021	0,000	8	
S132Y	0,020	0,001	11	> 0,999
L135I	0,022	0,001	7	> 0,999
F136L	0,022	0,001	5	> 0,999
E140M	0,021	0,001	7	> 0,999
A142T	0,021	0,001	7	> 0,999
G145A	0,075	0,003	8	< 0,001
R149Q	0,021	0,004	4	> 0,999
G178D	0,020	0,001	9	> 0,999
M184I	0,020	0,001	7	> 0,999
S185Y	0,021	0,001	13	> 0,999
Q186R	0,020	0,002	6	> 0,999
G4 (homo)	0,019	0,001	13	> 0,999

Note: Values with red text highlight statistically significant values. From: (Pelzmann, Hatab et al. 2022).

A simpler procedure was employed to examine mutations (E139K, R149P, G158S, G178D, and S185Y) that provided identifiable currents that were too small to allow application of the experimental paradigm described above, despite the maximum possible amounts of mRNA were injected: Firstly, basal and acetylcholine-induced currents were recorded as shown in Figure 8 under normal circumstances. Later, a reinterpretation with Na^+ in replacement of the entire K^+ inside the HK solution. Acetylcholine did not cause any measurable currents to be triggered during the reiteration with any of the above-mentioned mutations, therefore we can actually argue that these genetic mutations do not impact ion selectivity (data not shown).

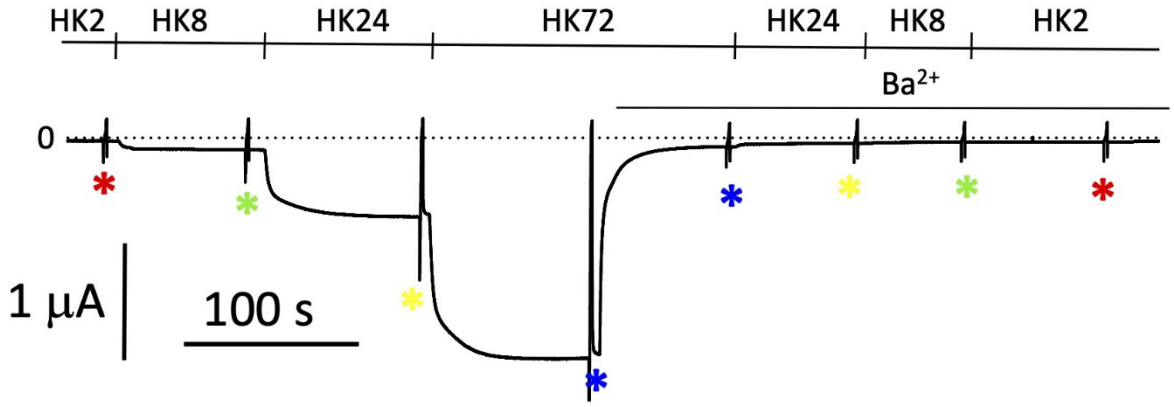

Figure 13

The P_{Na+}/P_{K+} ratio was estimated using an experimental paradigm as shown in the original current recording. -80 mV served as the holding potential. Above the current trace, superfusion with various extracellular media is highlighted. When recording the I/V relation, voltage ramps were applied at the moments identified by asterisks. From: (Pelzmann, Hatab et al. 2022).

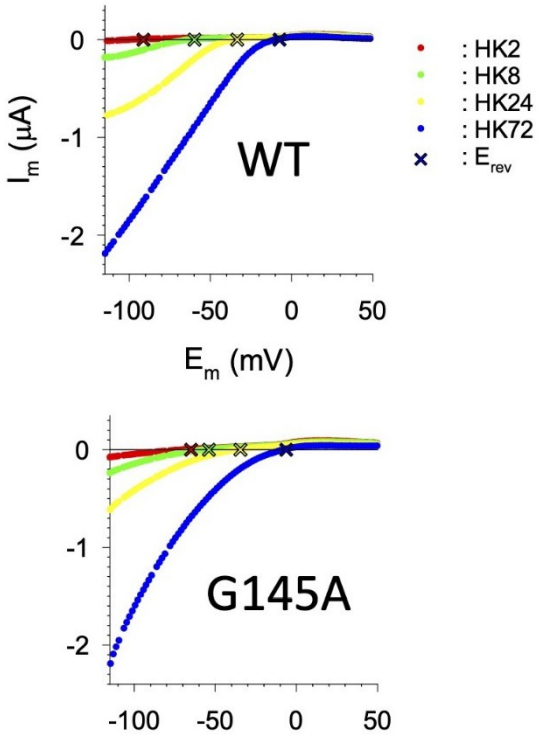

Figure 14

Representative I/V relations for $GIRK1^{WT}$/GIRK4 and $GIRK1^{G145A}$/GIRK4 are shown in the top and bottom graph, respectively. They were created by subtracting the current measured as a consequence of the voltage ramp in the addition of 2 mmol/L $Ba2^+$ from the ramp in the lack of $Ba2^+$ (red: HK2, green: HK8, yellow: HK24 and blue: HK72). Crosses signify the reversal potentials (Erev) of GIRK currents. From: (Pelzmann, Hatab et al. 2022).

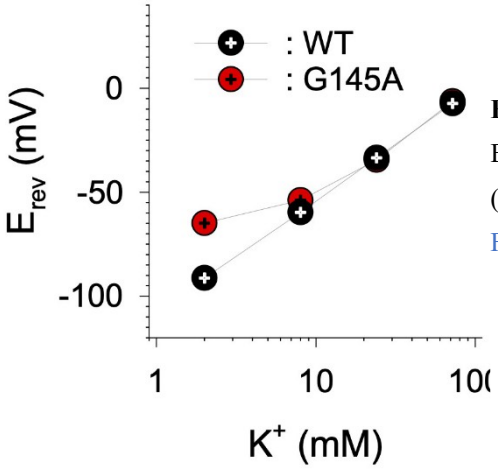

Figure 15: Representative of Reversal potentials (Erev)
Erev for GIRK1^{WT}/GIRK4 (black) and GIRK1^{G145A}/GIRK4 (red) measured at various extracellular K+ concentrations. From: (Pelzmann, Hatab et al. 2022).

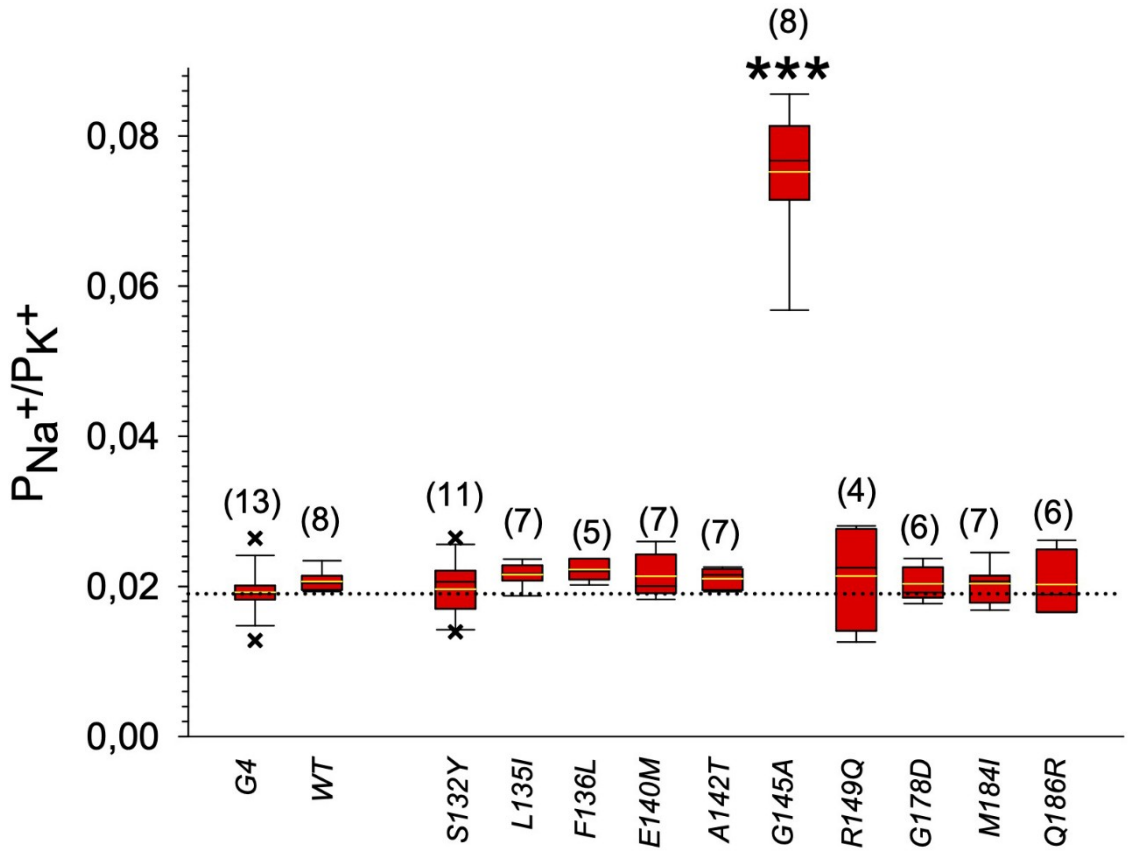

Figure 16: The P_{Na+}/P_{K+} ratio of the various mutations examined
The average values of the specified experimental group are shown as bars. Oocyte quantity is indicated in parentheses above the bars. A whisker indicates SEM. ***: At the p > 0.001 level, the mean value differs from GIRK1^{WT}/GIRK4 statistically significantly. From: (Pelzmann, Hatab et al. 2022).

4 Discussion

The data from this diploma thesis viably demonstrate that somatic missense mutations of GIRK1, which were confirmed in cancerous tumors, have profound effects on G-protein activated inwardly rectifying potassium channel gating and ion selectivity. In light of these phenotypic changes, one may recapitulate our current knowledge of human GIRK ion

channel dysfunction in disease. Numerous consequences for neurological, endocrine, and cardiac diseases have been linked to inherited and somatic mutations of the GIRKs-coding genes (Lüscher, Slesinger 2010, Mulatero, Monticone et al. 2013, Nolte, Munoz et al. 2017). We observed that G145A, which is situated right inside the ion selectivity filter of GIRK1 (Figure 7), causes reduced K^+ selectivity$_+$ of GIRK1/GIRK4 channels. Despite this effect being minor and far from a total loss of ion selectivity, this influence on ion selectivity is detectable. Therefore, it is uncertain whether the observed (roughly) threefold higher, but still modest, Na^+ permeation can have an impact in pathophysiology, having similar effect as somatic mutations of KCNJ5, which render GIRK channels permeable to Na^+ and result in altered GIRK expression and/or activation, causing primary aldosteronism (Shalomov, Handklo-Jamal et al. 2022). The vast bulk of the mutations examined in this thesis displayed phenotypes which can be classified into three groups: (i) normal/reduced expression along with reduced/absent function (S132Y, F136L, E139K, G145A, R149Q, R149P, G178D, S185Y, Q186R); (ii) normal/increased expression along with increased function (E140M, A142T, M184I); and (iii) minimal expression but greatly increased function (I151N, G158S). It has been recognized in the past that abnormally high expression levels of GIRK1, rather than somatic mutations, contribute to the development and spreading of breast tumors (Kammerer, Jahn et al. 2016, Kammerer, Sokolowski et al. 2016, Stringer, Cooper et al. 2001, Brevet, Ahidouch et al. 2008, Wagner, Stadelmeyer et al. 2010, Rezania, Kammerer et al. 2016, Schratter, Scheruebel et al. 2019). In accordance, primary breast cancers were found to be the least influenced by somatic mutations of KCNJ3 (Pelzmann, Hatab et al. 2022). Noticeably, functional effects of GIRK1 overexpression are comparable to those that arise from somatic mutations that result in the gain of function. Therefore, in primary tumors where somatic mutations of KCNJ3 occur often, gain of function mutations that are identical or functionally comparable to those studied here, may be implicated in the formation and development of malignant cancer. Hence, categories (ii) and (iii) are expected to have significant impact on pathophysiological outcome. Somatic mutations that are classified within group (i), are less likely to promote generation and/or development of cancer. The wide functional range of the studied somatic mutations should be emphasized. Even outside this range, mutations in the untranslated regions, which may potentially affect transcription were detected. Also, silent somatic mutations, which presumably exert little impact (this impact may, however, manifest itself via codon usage issues) and loss of function mutations (mostly frameshift mutations, and indeed group (i)) may have effects on carcinogenesis and cancer progression, but the impact is expected to be smaller compared to the gain of function mutations, which are identified here (groups (ii) and (iii)).

It will take additional, careful and targeted screening and compilation of somatic mutations in tumor samples in the context of histological parameters and tumor growth, along with further research into human cancer and cancer proliferation and differentiation, to comprehend whether somatic mutations in the KCNJ3 gene are indeed crucial in the clinical context.

Acceptance of participation and ethical clearance

The Medical University of Graz's Ethics Committee evaluated and granted the animal study.

References

1. NISHIDA, M., CADENE, M., CHAIT, B.T. and MACKINNON, R., 2007. Crystal structure of a Kir3.1-prokaryotic Kir channel chimera. *The EMBO journal,* **26**(17), pp. 4005-4015.

2. HANAHAN, D. and WEINBERG, R.A., 2000. The Hallmarks of Cancer. *Cell,* **100**(1), pp. 57-70.

3. HANAHAN, D. and WEINBERG, R.A., 2011. Hallmarks of Cancer: The Next Generation. *Cell,* **144**(5), pp. 646-674.

4. LOEB, L.A., 1991. Mutator Phenotype May Be Required for Multistage Carcinogenesis. *Cancer research,* **51**(12), pp. 3075-3079.

5. SALK, J.J., FOX, E.J. and LOEB, L.A., 2010. Mutational heterogeneity in human cancers: origin and consequences. *Annual review of pathology,* **5**, pp. 51-75.

6. NEGRINI, S., GORGOULIS, V.G. and HALAZONETIS, T.D., 2010. Genomic instability — an evolving hallmark of cancer. *Nature Reviews Molecular Cell Biology,* **11**(3), pp. 220-228.

7. SIGAL, A. and ROTTER, V., 2000. Oncogenic Mutations of the p53 Tumor Suppressor: The Demons of the Guardian of the Genome. *Cancer research,* **60**(24), pp. 6788-6793.

8. KASTAN, M.B., 2008. DNA Damage Responses: Mechanisms and Roles in Human Disease. *Molecular Cancer Research,* **6**(4), pp. 517-524.

9. JACKSON, S.P. and BARTEK, J., 2009. The DNA-damage response in human biology and disease. *Nature,* **461**(7267), pp. 1071-1078.

10. KINZLER, K.W. and VOGELSTEIN, B., 1997. Gatekeepers and caretakers. *Nature,* **386**(6627), pp. 761-763.

11. LEVINE, A.J., 1997. p53, the Cellular Gatekeeper for Growth and Division. *Cell,* **88**(3), pp. 323-331.

12. LANE, D.P., 1992. p53, guardian of the genome. *Nature,* **358**(6381), pp. 15-16.

13. HOLMGREN, L., SZELES, A., RAJNAVÖLGYI, E., FOLKMAN, J., KLEIN, G., ERNBERG, I. and FALK, K.I., 1999. Horizontal Transfer of DNA by the Uptake of Apoptotic Bodies. *Blood,* **93**(11), pp. 3956-3963.

14. ESTELLER, M., 2007. Cancer epigenomics: DNA methylomes and histone-modification maps. *Nature Reviews Genetics,* **8**(4), pp. 286-298.

15. JONES, P.A. and BAYLIN, S.B., 2007. The epigenomics of cancer. *Cell,* **128**(4), pp. 683-692.

16. BERDASCO, M. and ESTELLER, M., 2010. Aberrant Epigenetic Landscape in Cancer: How Cellular Identity Goes Awry. *Developmental Cell,* **19**(5), pp. 698-711.

17. ARTANDI, S.E. and DEPINHO, R.A., 2010. Telomeres and telomerase in cancer. *Carcinogenesis,* **31**(1), pp. 9-18.

18. KORKOLA, J. and GRAY, J.W., 2010. Breast cancer genomes—form and function. *Current opinion in genetics & development,* **20**(1), pp. 4-14.

19. YAMASHITA, N., HAMADA, H., TSURUO, T. and OGATA, E., 1987. Enhancement of voltage-gated Na+ channel current associated with multidrug resistance in human leukemia cells. *Cancer research,* **47**(14), pp. 3736-3741.

20. LEE, S.C., DEUTSCH, C. and BECK, W.T., 1988. Comparison of ion channels in multidrug-resistant and -sensitive human leukemic cells. *Proceedings of the National Academy of Sciences,* **85**(6), pp. 2019-2023.

21. PANCRAZIO, J.J., VIGLIONE, M.P., TABBARA, I.A. and KIM, Y.I., 1989. Voltage-dependent ion channels in small-cell lung cancer cells. *Cancer research,* **49**(21), pp. 5901-5906.

22. BATRA, S. and ALENFALL, J., 1991. Effect of diverse categories of drugs on Human Colon tumour cell proliferation. *Anticancer Research,* **11**, pp. 1221-4.

23. TAYLOR, J.M. and SIMPSON, R.U., 1992. Inhibition of cancer cell growth by calcium channel antagonists in the athymic mouse. *Cancer research,* **52**(9), pp. 2413-2418.

24. PANCRAZIO, J.J., TABBARA, I.A. and KIM, Y.I., 1993. Voltage-activated K+ conductance and cell proliferation in small-cell lung cancer. *Anticancer Research,* **13**(4), pp. 1231-1234.

25. PREVARSKAYA, N., SKRYMA, R. and SHUBA, Y., 2010. Ion channels and the hallmarks of cancer. *Trends in molecular medicine,* **16**(3), pp. 107-121.

26. HUBER, S.M., 2013. Oncochannels. *Cell calcium,* **53**(4), pp. 241-255.

27. LITAN, A. and LANGHANS, S.A., 2015. Cancer as a channelopathy: ion channels and pumps in tumor development and progression. *Frontiers in cellular neuroscience,* **9**.

28. LÜSCHER, C. and SLESINGER, P.A., 2010. Emerging roles for G protein-gated inwardly rectifying potassium (GIRK) channels in health and disease. *Nature Reviews Neuroscience,* **11**(5), pp. 301-315.

29. TAKANAMI, I., INOUE, Y. and GIKA, M., 2004. G-protein inwardly rectifying potassium channel 1 (GIRK 1) gene expression correlates with tumor progression in non-small cell lung cancer. *BMC Cancer,* **4**(1), pp. 79.

30. BREVET, M., FUCKS, D., CHATELAIN, D., REGIMBEAU, J., DELCENSERIE, R., SEVESTRE, H. and OUADID-AHIDOUCH, H., 2009. Deregulation of 2 Potassium Channels in Pancreas Adenocarcinomas: Implication of KV1.3 Gene Promoter Methylation. *Pancreas,* **38**(6),.

31. STRINGER, B.K., COOPER, A.G. and SHEPARD, S.B., 2001. Overexpression of the G-protein inwardly rectifying potassium channel 1 (GIRK1) in primary breast carcinomas correlates with axillary lymph node metastasis. *Cancer research,* **61**(2), pp. 582-588.

32. BREVET, M., AHIDOUCH, A., SEVESTRE, H., MERVIEL, P., EL HIANI, Y., ROBBE, M. and OUADID-AHIDOUCH, H., 2008. Expression of K+ channels in normal and cancerous human breast. *Histology and histopathology,* **23**(8), pp. 965-972.

33. REZANIA, S., KAMMERER, S., LI, C., STEINECKER-FROHNWIESER, B., GORISCHEK, A., DEVANEY, T.T.J., VERHEYEN, S., PASSEGGER, C.A.,

TABRIZI-WIZSY, N., HACKL, H., PLATZER, D., ZARNANI, A.H., MALLE, E., JAHN, S.W., BAUERNHOFER, T. and SCHREIBMAYER, W., 2016. Overexpression of KCNJ3 gene splice variants affects vital parameters of the malignant breast cancer cell line MCF-7 in an opposing manner. *BMC Cancer,* **16**(1), pp. 628.

34. KO, J., KO, E.A., GU, W., LIM, I., BANG, H. and ZHOU, T., 2013. Expression profiling of ion channel genes predicts clinical outcome in breast cancer. *Molecular Cancer,* **12**(1), pp. 106.

35. KAMMERER, S., SOKOLOWSKI, A., HACKL, H., PLATZER, D., WENZEL JAHN, S., EL-HELIEBI, A., SCHWARZENBACHER, D., STIEGELBAUER, V., PICHLER, M., REZANIA, S., FIEGL, H., PEINTINGER, F., REGITNIG, P., HOEFLER, G., SCHREIBMAYER, W. and BAUERNHOFER, T., 2016. KCNJ3 is a new independent prognostic marker for estrogen receptor positive breast cancer patients. *Oncotarget; Vol 7, No 51, .*

36. JING, J., CHIKVASHVILI, D., SINGER-LAHAT, D., THORNHILL, W.B., REUVENY, E. and LOTAN, I., 1999. Fast inactivation of a brain K+ channel composed of Kv1.1 and Kvbeta1.1 subunits modulated by G protein beta gamma subunits. *The EMBO journal,* **18**(5), pp. 1245-1256.

37. WAGNER, V., STADELMEYER, E., RIEDERER, M., REGITNIG, P., GORISCHEK, A., DEVANEY, T., SCHMIDT, K., TRITTHART, H.A., HIRSCHBERG, K., BAUERNHOFER, T. and SCHREIBMAYER, W., 2010. Cloning and characterisation of GIRK1 variants resulting from alternative RNA editing of the KCNJ3 gene transcript in a human breast cancer cell line. *Journal of cellular biochemistry,* **110**(3), pp. 598-608.

38. TREIBER, F., ROSKER, C., KEREN-RAIFMAN, T., STEINECKER, B., GORISCHEK, A., DASCAL, N. and SCHREIBMAYER, W., 2013. Molecular basis of the facilitation of the heterooligomeric GIRK1/GIRK4 complex by cAMP dependent protein kinase. *Biochimica et biophysica acta,* **1828**(4), pp. 1214-1221.

39. HEDIN, K.E., LIM, N.F. and CLAPHAM, D.E., 1996. Cloning of a Xenopus laevis inwardly rectifying K+ channel subunit that permits GIRK1 expression of IKACh currents in oocytes. *Neuron,* **16**(2), pp. 423-429.

40. SCHREIBMAYER, W., LESTER, H.A. and DASCAL, N., 1994. Voltage clamping of Xenopus laevis oocytes utilizing agarose-cushion electrodes. *Pflugers Archiv : European journal of physiology,* **426**(5), pp. 453-458.

41. SHALOMOV, B., HANDKLO-JAMAL, R., REDDY, H.P., THEODOR, N., BERA, A.K. and DASCAL, N., 2022. A revised mechanism of action of hyperaldosteronism-linked mutations in cytosolic domains of GIRK4 (KCNJ5). *The Journal of physiology,* **600**(6), pp. 1419-1437.

42. MULATERO, P., MONTICONE, S., RAINEY, W.E., VEGLIO, F. and WILLIAMS, T.A., 2013. Role of KCNJ5 in familial and sporadic primary aldosteronism. *Nature reviews.Endocrinology,* **9**(2), pp. 104-112.

43. CHAN, K.W., SUI, J.L., VIVAUDOU, M. and LOGOTHETIS, D.E., 1996. Control of channel activity through a unique amino acid residue of a G protein-gated inwardly rectifying K+ channel subunit. *Proceedings of the National Academy of Sciences of the United States of America,* **93**(24), pp. 14193-14198.

44. MAO, J., WANG, X., CHEN, F., WANG, R., ROJAS, A., SHI, Y., PIAO, H. and JIANG, C., 2004. Molecular basis for the inhibition of G protein-coupled inward rectifier K(+) channels by protein kinase C. *Proceedings of the National Academy of Sciences of the United States of America,* **101**(4), pp. 1087-1092.

45. PELZMANN, B., HATAB, A., SCHERUEBEL, S., LANGTHALER, S., RIENMUELLER, T., SOKOLOWSKI, A., GORISCHEK, A., PLATZER, D., ZORN-PAULY, K., JAHN, S.W., BAUERNHOFER, T. and SCHREIBMAYER, W., 2022. Consequences of somatic mutations of GIRK1 detected in primary malign tumors on expression and function of G-protein activated, inwardly rectifying, K(+) channels. *Frontiers in oncology,* **12**, pp. 998907.

46. NOLTE, I.M., MUNOZ, M.L., TRAGANTE, V., AMARE, A.T., JANSEN, R., VAEZ, A., VON DER HEYDE, B., AVERY, C.L., BIS, J.C., DIERCKX, B., VAN DONGEN, J., GOGARTEN, S.M., GOYETTE, P., HERNESNIEMI, J., HUIKARI, V., HWANG, S., JAJU, D., KERR, K.F., KLUTTIG, A., KRIJTHE, B.P., KUMAR, J., VAN DER LAAN, SANDER W, LYYTIKAINEN, L., MAIHOFER, A.X., MINASSIAN, A., VAN DER MOST, PETER J, MULLER-NURASYID, M., NIVARD, M., SALVI, E., STEWART, J.D., THAYER, J.F., VERWEIJ, N., WONG,

A., ZABANEH, D., ZAFARMAND, M.H., ABDELLAOUI, A., ALBARWANI, S., ALBERT, C., ALONSO, A., ASHAR, F., AUVINEN, J., AXELSSON, T., BAKER, D.G., DE BAKKER, PAUL I W, BARCELLA, M., BAYOUMI, R., BIERINGA, R.J., BOOMSMA, D., BOUCHER, G., BRITTON, A.R., CHRISTOPHERSEN, I., DIETRICH, A., EHRET, G.B., ELLINOR, P.T., ESKOLA, M., FELIX, J.F., FLORAS, J.S., FRANCO, O.H., FRIBERG, P., GADEMAN, M.G.J., GEYER, M.A., GIEDRAITIS, V., HARTMAN, C.A., HEMERICH, D., HOFMAN, A., HOTTENGA, J., HUIKURI, H., HUTRI-KAHONEN, N., JOUVEN, X., JUNTTILA, J., JUONALA, M., KIVINIEMI, A.M., KORS, J.A., KUMARI, M., KUZNETSOVA, T., LAURIE, C.C., LEFRANDT, J.D., LI, Y., LI, Y., LIAO, D., LIMACHER, M.C., LIN, H.J., LINDGREN, C.M., LUBITZ, S.A., MAHAJAN, A., MCKNIGHT, B., ZU SCHWABEDISSEN, H.M., MILANESCHI, Y., MONONEN, N., MORRIS, A.P., NALLS, M.A., NAVIS, G., NEIJTS, M., NIKUS, K., NORTH, K.E., O'CONNOR, D.T., ORMEL, J., PERZ, S., PETERS, A., PSATY, B.M., RAITAKARI, O.T., RISBROUGH, V.B., SINNER, M.F., SISCOVICK, D., SMIT, J.H., SMITH, N.L., SOLIMAN, E.Z., SOTOODEHNIA, N., STAESSEN, J.A., STEIN, P.K., STILP, A.M., STOLARZ-SKRZYPEK, K., STRAUCH, K., SUNDSTROM, J., SWENNE, C.A., SYVANEN, A., TARDIF, J., TAYLOR, K.D., TEUMER, A., THORNTON, T.A., TINKER, L.E., UITTERLINDEN, A.G., VAN SETTEN, J., VOSS, A., WALDENBERGER, M., WILHELMSEN, K.C., WILLEMSEN, G., WONG, Q., ZHANG, Z., ZONDERMAN, A.B., CUSI, D., EVANS, M.K., GREISER, H.K., VAN DER HARST, P., HASSAN, M., INGELSSON, E., JARVELIN, M., KAAB, S., KAHONEN, M., KIVIMAKI, M., KOOPERBERG, C., KUH, D., LEHTIMAKI, T., LIND, L., NIEVERGELT, C.M., O'DONNELL, C.J., OLDEHINKEL, A.J., PENNINX, B., REINER, A.P., RIESE, H., VAN ROON, A.M., RIOUX, J.D., ROTTER, J.I., SOFER, T., STRICKER, B.H., TIEMEIER, H., VRIJKOTTE, T.G.M., ASSELBERGS, F.W., BRUNDEL, BIANCA J J M, HECKBERT, S.R., WHITSEL, E.A., DEN HOED, M., SNIEDER, H. and DE GEUS, ECO J C, 2017. Genetic loci associated with heart rate variability and their effects on cardiac disease risk. *Nature communications,* **8**, pp. 15805.

47. KAMMERER, S., JAHN, S.W., WINTER, E., EIDENHAMMER, S., REZANIA, S., REGITNIG, P., PICHLER, M., SCHREIBMAYER, W. and BAUERNHOFER, T., 2016. Critical evaluation of *KCNJ3* gene product detection in human breast cancer: mRNA in situ hybridisation is superior to immunohistochemistry. *J Clin Pathol,* **69**(12), pp. 1116.

48. SCHRATTER, G., SCHERUEBEL, S., LANGTHALER, S., ESTER, K., PELZMANN, B., GHAFFARI-TABRIZI-WIZSY, N., REZANIA, S., GORISCHEK, A., PLATZER, D., ZORN-PAULY, K., AHAMMER, H., PROKESCH, A., STANZER, S., DEVANEY, T.T.J., SCHMIDT, K., JAHN, S.W., PRASSL, R., BAUERNHOFER, T. and SCHREIBMAYER, W., 2019. GIRK1 triggers multiple cancer-related pathways in the benign mammary epithelial cell line MCF10A. *Scientific reports,* **9**(1), pp. 19277-w.

Index

Table 3: List of somatic mutations of the KCNJ3 gene in primary malignant tumors as listed in https://portal.gdc.cancer.gov/exploration

DNA Change	Type	Consequences	# Cases in Cohort	# Cases Across the GDC
chr2:g.154854785delT	Deletion	Frameshift KCNJ3 P329Lfs*2	4 / 305, 1.31%	4 / 13,714
chr2:g.154699308G>A	Substitution	Missense KCNJ3 G178D	3 / 305, 0.98%	3 / 13,714
chr2:g.154699189C>T	Substitution	Synonymous KCNJ3 I138=	3 / 305, 0.98%	3 / 13,714
chr2:g.154709629C>T	Substitution	Synonymous KCNJ3 F243=	2 / 305, 0.66%	2 / 13,714
chr2:g.154698983G>T	Substitution	Missense KCNJ3 D70Y	2 / 305, 0.66%	2 / 13,714
chr2:g.154709654G>A	Substitution	Missense KCNJ3 D252N	2 / 305, 0.66%	2 / 13,714
chr2:g.154855052A>G	Substitution	Synonymous KCNJ3 K415=	2 / 305, 0.66%	2 / 13,714
chr2:g.154855137C>T	Substitution	Missense KCNJ3 P444S	2 / 305, 0.66%	2 / 13,714
chr2:g.154709696T>C	Substitution	Missense KCNJ3 S266P	2 / 305, 0.66%	2 / 13,714
chr2:g.154709690C>A	Substitution	Missense KCNJ3 L264I	2 / 305, 0.66%	2 / 13,714
chr2:g.154855055C>A	Substitution	Synonymous KCNJ3 L416=	2 / 305, 0.66%	2 / 13,714
chr2:g.154855302C>T	Substitution	Missense KCNJ3 R499C	2 / 305, 0.66%	2 / 13,714
chr2:g.154855101G>A	Substitution	Missense KCNJ3 D432N	2 / 305, 0.66%	2 / 13,714
chr2:g.154854771C>A	Substitution	Missense KCNJ3 L322I	2 / 305, 0.66%	2 / 13,714
chr2:g.154699374C>T	Substitution	Missense KCNJ3 A200V	2 / 305, 0.66%	2 / 13,714
chr2:g.154854934T>C	Substitution	Missense KCNJ3 I376T	2 / 305, 0.66%	2 / 13,714
chr2:g.154855123G>A	Substitution	Missense KCNJ3 R439Q	2 / 305, 0.66%	2 / 13,714
chr2:g.154699346G>A	Substitution	Missense KCNJ3 A191T	2 / 305, 0.66%	2 / 13,714
chr2:g.154855134G>C	Substitution	Missense KCNJ3 V443L	2 / 305, 0.66%	2 / 13,714
chr2:g.154854881G>A	Substitution	Synonymous KCNJ3 V358=	2 / 305, 0.66%	2 / 13,714
chr2:g.154855046C>T	Substitution	Synonymous KCNJ3 P413=	2 / 305, 0.66%	2 / 13,714
chr2:g.154699100C>T	Substitution	Missense KCNJ3 R109W	2 / 305, 0.66%	2 / 13,714
chr2:g.154709723G>A	Substitution	Missense KCNJ3 D275N	2 / 305, 0.66%	2 / 13,714
chr2:g.154855119C>T	Substitution	Stop Gained KCNJ3 Q438*	2 / 305, 0.66%	2 / 13,714
chr2:g.154699345C>T	Substitution	Synonymous KCNJ3 R190=	2 / 305, 0.66%	2 / 13,714
chr2:g.154854745G>A	Substitution	Missense KCNJ3 R313Q	2 / 305, 0.66%	2 / 13,714
chr2:g.154854961C>A	Substitution	Missense KCNJ3 S385Y	2 / 305, 0.66%	2 / 13,714
chr2:g.154855097G>T	Substitution	Missense KCNJ3 L430F	2 / 305, 0.66%	2 / 13,714
chr2:g.154698789G>A	Substitution	Missense KCNJ3 R5Q	2 / 305, 0.66%	2 / 13,714
chr2:g.154698981C>G	Substitution	Missense KCNJ3 S69W	2 / 305, 0.66%	2 / 13,714
chr2:g.154699091G>A	Substitution	Missense KCNJ3 A106T	2 / 305, 0.66%	2 / 13,714

chr2:g.154857271delA	Deletion	3 Prime UTR KCNJ3	2 / 305, 0.66%	2 / 13,714
chr2:g.154709757G>A	Substitution	Missense KCNJ3 R286Q	2 / 305, 0.66%	2 / 13,714
chr2:g.154699071C>T	Substitution	Missense KCNJ3 A99V	2 / 305, 0.66%	2 / 13,714
chr2:g.154709621G>A	Substitution	Missense KCNJ3 G241S	2 / 305, 0.66%	2 / 13,714
chr2:g.154855159T>A	Substitution	Missense KCNJ3 L451Q	1 / 305, 0.33%	1 / 13,714
chr2:g.154855339A>C	Substitution	3 Prime UTR KCNJ3	1 / 305, 0.33%	1 / 13,714
chr2:g.154854931C>A	Substitution	Missense KCNJ3 A375D	1 / 305, 0.33%	1 / 13,714
chr2:g.154855303G>A	Substitution	Missense KCNJ3 R499H	1 / 305, 0.33%	1 / 13,714
chr2:g.154854844A>G	Substitution	Missense KCNJ3 H346R	1 / 305, 0.33%	1 / 13,714
chr2:g.154699264C>A	Substitution	Synonymous KCNJ3 L163=	1 / 305, 0.33%	1 / 13,714
chr2:g.154699309C>A	Substitution	Synonymous KCNJ3 G178=	1 / 305, 0.33%	1 / 13,714
chr2:g.154855024T>A	Substitution	Missense KCNJ3 I406N	1 / 305, 0.33%	1 / 13,714
chr2:g.154699276C>T	Substitution	Synonymous KCNJ3 I167=	1 / 305, 0.33%	1 / 13,714
chr2:g.154699165C>T	Substitution	Synonymous KCNJ3 F130=	1 / 305, 0.33%	1 / 13,714
chr2:g.154855254A>G	Substitution	Missense KCNJ3 R483G	1 / 305, 0.33%	1 / 13,714
chr2:g.154699404C>T	Substitution	Missense KCNJ3 T210M	1 / 305, 0.33%	1 / 13,714
chr2:g.154856600G>A	Substitution	3 Prime UTR KCNJ3	1 / 305, 0.33%	1 / 13,714
chr2:g.154699053T>A	Substitution	Missense KCNJ3 V93E	1 / 305, 0.33%	1 / 13,714
chr2:g.154854866C>A	Substitution	Synonymous KCNJ3 T353=	1 / 305, 0.33%	1 / 13,714
chr2:g.154709660G>T	Substitution	Missense KCNJ3 G254C	1 / 305, 0.33%	1 / 13,714
chr2:g.154854843C>T	Substitution	Missense KCNJ3 H346Y	1 / 305, 0.33%	1 / 13,714
chr2:g.154855137C>A	Substitution	Missense KCNJ3 P444T	1 / 305, 0.33%	1 / 13,714
chr2:g.154699249C>A	Substitution	Synonymous KCNJ3 G158=	1 / 305, 0.33%	1 / 13,714
chr2:g.154854900C>T	Substitution	Missense KCNJ3 L365F	1 / 305, 0.33%	1 / 13,714
chr2:g.154855269C>T	Substitution	Missense KCNJ3 L488F	1 / 305, 0.33%	1 / 13,714
chr2:g.154855161G>A	Substitution	Missense KCNJ3 V452I	1 / 305, 0.33%	1 / 13,714
chr2:g.154698889G>T	Substitution	Synonymous KCNJ3 V38=	1 / 305, 0.33%	1 / 13,714
chr2:g.154854838A>C	Substitution	Missense KCNJ3 Q344P	1 / 305, 0.33%	1 / 13,714
chr2:g.154709682A>C	Substitution	Missense KCNJ3 Q261P	1 / 305, 0.33%	1 / 13,714
chr2:g.154855097delG	Deletion	Frameshift KCNJ3 G431Efs*5	1 / 305, 0.33%	1 / 13,714
chr2:g.154854910C>T	Substitution	Missense KCNJ3 S368L	1 / 305, 0.33%	1 / 13,714
chr2:g.154854948G>T	Substitution	Stop Gained KCNJ3 E381*	1 / 305, 0.33%	1 / 13,714
chr2:g.154699148G>T	Substitution	Missense KCNJ3 A125S	1 / 305, 0.33%	1 / 13,714
chr2:g.154855019G>A	Substitution	Synonymous KCNJ3 Q404=	1 / 305, 0.33%	1 / 13,714
chr2:g.154709745A>G	Substitution	Missense KCNJ3 D282G	1 / 305, 0.33%	1 / 13,714
chr2:g.154698941C>A	Substitution	Missense KCNJ3 Q56K	1 / 305, 0.33%	1 / 13,714

chr2:g.154855156A>T	Substitution	Missense KCNJ3 K450I	1 / 305, 0.33%	1 / 13,714
chr2:g.154698871C>A	Substitution	Missense KCNJ3 D32E	1 / 305, 0.33%	1 / 13,714
chr2:g.154698793G>A	Substitution	Synonymous KCNJ3 R6=	1 / 305, 0.33%	1 / 13,714
chr2:g.154699194C>T	Substitution	Missense KCNJ3 T140M	1 / 305, 0.33%	1 / 13,714
chr2:g.154855140G>T	Substitution	Missense KCNJ3 G445C	1 / 305, 0.33%	1 / 13,714
chr2:g.154855000A>G	Substitution	Missense KCNJ3 K398R	1 / 305, 0.33%	1 / 13,714
chr2:g.154855186C>A	Substitution	Missense KCNJ3 S460Y	1 / 305, 0.33%	1 / 13,714
chr2:g.154855090A>G	Substitution	Missense KCNJ3 Y428C	1 / 305, 0.33%	1 / 13,714
chr2:g.154698805C>A	Substitution	Missense KCNJ3 D10E	1 / 305, 0.33%	1 / 13,714
chr2:g.154709624G>A	Substitution	Missense KCNJ3 E242K	1 / 305, 0.33%	1 / 13,714
chr2:g.154709706C>T	Substitution	Missense KCNJ3 T269I	1 / 305, 0.33%	1 / 13,714
chr2:g.154698837G>T	Substitution	Missense KCNJ3 G21V	1 / 305, 0.33%	1 / 13,714
chr2:g.154857050T>C	Substitution	3 Prime UTR KCNJ3	1 / 305, 0.33%	1 / 13,714
chr2:g.154855124A>G	Substitution	Synonymous KCNJ3 R439=	1 / 305, 0.33%	1 / 13,714
chr2:g.154854903C>A	Substitution	Missense KCNJ3 L366I	1 / 305, 0.33%	1 / 13,714
chr2:g.154854981C>T	Substitution	Synonymous KCNJ3 L392=	1 / 305, 0.33%	1 / 13,714
chr2:g.154699242C>A	Substitution	Missense KCNJ3 P156H	1 / 305, 0.33%	1 / 13,714
chr2:g.154699201C>A	Substitution	Synonymous KCNJ3 A142=	1 / 305, 0.33%	1 / 13,714
chr2:g.154698875C>G	Substitution	Missense KCNJ3 Q34E	1 / 305, 0.33%	1 / 13,714
chr2:g.154709722C>T	Substitution	Synonymous KCNJ3 I274=	1 / 305, 0.33%	1 / 13,714
chr2:g.154854792C>T	Substitution	Missense KCNJ3 P329S	1 / 305, 0.33%	1 / 13,714
chr2:g.154699294C>T	Substitution	Synonymous KCNJ3 D173=	1 / 305, 0.33%	1 / 13,714
chr2:g.154698895G>A	Substitution	Synonymous KCNJ3 K40=	1 / 305, 0.33%	1 / 13,714
chr2:g.154699269A>T	Substitution	Missense KCNJ3 Q165L	1 / 305, 0.33%	1 / 13,714
chr2:g.154699106G>A	Substitution	Missense KCNJ3 D111N	1 / 305, 0.33%	1 / 13,714
chr2:g.154699390G>A	Substitution	Synonymous KCNJ3 R205=	1 / 305, 0.33%	1 / 13,714
chr2:g.154855147C>G	Substitution	Stop Gained KCNJ3 S447*	1 / 305, 0.33%	1 / 13,714
chr2:g.154855297C>A	Substitution	Missense KCNJ3 S497Y	1 / 305, 0.33%	1 / 13,714
chr2:g.154854828G>T	Substitution	Missense KCNJ3 D341Y	1 / 305, 0.33%	1 / 13,714
chr2:g.154855167delA	Deletion	Frameshift KCNJ3 T455Pfs*9	1 / 305, 0.33%	1 / 13,714
chr2:g.154699178C>A	Substitution	Missense KCNJ3 L135I	1 / 305, 0.33%	1 / 13,714
chr2:g.154855175C>T	Substitution	Synonymous KCNJ3 T456=	1 / 305, 0.33%	1 / 13,714
chr2:g.154709635C>A	Substitution	Synonymous KCNJ3 P245=	1 / 305, 0.33%	1 / 13,714
chr2:g.154699145G>A	Substitution	Missense KCNJ3 V124M	1 / 305, 0.33%	1 / 13,714
chr2:g.154855058G>C	Substitution	Missense KCNJ3 L417F	1 / 305, 0.33%	1 / 13,714
chr2:g.154699220C>T	Substitution	Stop Gained KCNJ3 R149*	1 / 305, 0.33%	1 / 13,714

chr2:g.154855092A>T	Substitution	Missense KCNJ3 S429C	1 / 305, 0.33%	1 / 13,714
chr2:g.154709672G>T	Substitution	Missense KCNJ3 G258W	1 / 305, 0.33%	1 / 13,714
chr2:g.154698931G>T	Substitution	Synonymous KCNJ3 R52=	1 / 305, 0.33%	1 / 13,714
chr2:g.154699272C>T	Substitution	Missense KCNJ3 S166F	1 / 305, 0.33%	1 / 13,714
chr2:g.154699066C>T	Substitution	Synonymous KCNJ3 F97=	1 / 305, 0.33%	1 / 13,714
chr2:g.154854734T>G	Substitution	Synonymous KCNJ3 T309=	1 / 305, 0.33%	1 / 13,714
chr2:g.154699227T>A	Substitution	Missense KCNJ3 I151N	1 / 305, 0.33%	1 / 13,714
chr2:g.154854818C>A	Substitution	Missense KCNJ3 F337L	1 / 305, 0.33%	1 / 13,714
chr2:g.154699228C>A	Substitution	Synonymous KCNJ3 I151=	1 / 305, 0.33%	1 / 13,714
chr2:g.154855046_154855047insA	Insertion	Frameshift KCNJ3 L416Tfs*39	1 / 305, 0.33%	1 / 13,714
chr2:g.154699332A>G	Substitution	Missense KCNJ3 Q186R	1 / 305, 0.33%	1 / 13,714
chr2:g.154854729A>G	Substitution	Missense KCNJ3 M308V	1 / 305, 0.33%	1 / 13,714
chr2:g.154855112G>A	Substitution	Missense KCNJ3 M435I	1 / 305, 0.33%	1 / 13,714
chr2:g.154855122C>T	Substitution	Stop Gained KCNJ3 R439*	1 / 305, 0.33%	1 / 13,714
chr2:g.154698826A>G	Substitution	Synonymous KCNJ3 T17=	1 / 305, 0.33%	1 / 13,714
chr2:g.154709666A>T	Substitution	Missense KCNJ3 S256C	1 / 305, 0.33%	1 / 13,714
chr2:g.154698867A>T	Substitution	Missense KCNJ3 Q31L	1 / 305, 0.33%	1 / 13,714
chr2:g.154709604delC	Deletion	Frameshift KCNJ3 S235Ffs*19	1 / 305, 0.33%	1 / 13,714
chr2:g.154855246G>A	Substitution	Missense KCNJ3 G480E	1 / 305, 0.33%	1 / 13,714
chr2:g.154855346G>A	Substitution	3 Prime UTR KCNJ3	1 / 305, 0.33%	1 / 13,714
chr2:g.154855263G>A	Substitution	Missense KCNJ3 G486R	1 / 305, 0.33%	1 / 13,714
chr2:g.154709716C>T	Substitution	Synonymous KCNJ3 H272=	1 / 305, 0.33%	1 / 13,714
chr2:g.154699450C>T	Substitution	Synonymous KCNJ3 S225=	1 / 305, 0.33%	1 / 13,714
chr2:g.154698912T>C	Substitution	Missense KCNJ3 F46S	1 / 305, 0.33%	1 / 13,714
chr2:g.154699277C>A	Substitution	Missense KCNJ3 L168M	1 / 305, 0.33%	1 / 13,714
chr2:g.154854753T>A	Substitution	Missense KCNJ3 Y316N	1 / 305, 0.33%	1 / 13,714
chr2:g.154855103_154855104insT	Insertion	Frameshift KCNJ3 L433Ffs*22	1 / 305, 0.33%	1 / 13,714
chr2:g.154854922T>A	Substitution	Missense KCNJ3 I372K	1 / 305, 0.33%	1 / 13,714
chr2:g.154698971C>T	Substitution	Missense KCNJ3 R66C	1 / 305, 0.33%	1 / 13,714
chr2:g.154855045C>T	Substitution	Missense KCNJ3 P413L	1 / 305, 0.33%	1 / 13,714
chr2:g.154699267C>T	Substitution	Synonymous KCNJ3 F164=	1 / 305, 0.33%	1 / 13,714
chr2:g.154709796T>C	Substitution	Missense KCNJ3 L299P	1 / 305, 0.33%	1 / 13,714
chr2:g.154699242C>T	Substitution	Missense KCNJ3 P156L	1 / 305, 0.33%	1 / 13,714
chr2:g.154709607G>T	Substitution	Missense KCNJ3 R236L	1 / 305, 0.33%	1 / 13,714
chr2:g.154699264C>G	Substitution	Synonymous KCNJ3 L163=	1 / 305, 0.33%	1 / 13,714
chr2:g.154855186C>T	Substitution	Missense KCNJ3 S460F	1 / 305, 0.33%	1 / 13,714

chr2:g.154854771C>T	Substitution	Missense KCNJ3 L322F	1 / 305, 0.33%	1 / 13,714
chr2:g.154857554A>C	Substitution	3 Prime UTR KCNJ3	1 / 305, 0.33%	1 / 13,714
chr2:g.154854784_154854785insT	Insertion	Frameshift KCNJ3 P329Sfs*11	1 / 305, 0.33%	1 / 13,714
chr2:g.154855152G>T	Substitution	Stop Gained KCNJ3 E449*	1 / 305, 0.33%	1 / 13,714
chr2:g.154699329C>A	Substitution	Missense KCNJ3 S185Y	1 / 305, 0.33%	1 / 13,714
chr2:g.154856365C>A	Substitution	3 Prime UTR KCNJ3	1 / 305, 0.33%	1 / 13,714
chr2:g.154854910C>A	Substitution	Stop Gained KCNJ3 S368*	1 / 305, 0.33%	1 / 13,714
chr2:g.154709606C>T	Substitution	Missense KCNJ3 R236W	1 / 305, 0.33%	1 / 13,714
chr2:g.154698815G>T	Substitution	Missense KCNJ3 V14L	1 / 305, 0.33%	1 / 13,714
chr2:g.154699105C>T	Substitution	Synonymous KCNJ3 G110=	1 / 305, 0.33%	1 / 13,714
chr2:g.154699010A>C	Substitution	Missense KCNJ3 K79Q	1 / 305, 0.33%	1 / 13,714
chr2:g.154855085A>G	Substitution	Synonymous KCNJ3 K426=	1 / 305, 0.33%	1 / 13,714
chr2:g.154699389G>T	Substitution	Missense KCNJ3 R205M	1 / 305, 0.33%	1 / 13,714
chr2:g.154699308G>T	Substitution	Missense KCNJ3 G178V	1 / 305, 0.33%	1 / 13,714
chr2:g.154855069C>T	Substitution	Missense KCNJ3 S421F	1 / 305, 0.33%	1 / 13,714
chr2:g.154854731G>C	Substitution	Missense KCNJ3 M308I	1 / 305, 0.33%	1 / 13,714
chr2:g.154699051C>G	Substitution	Synonymous KCNJ3 T92=	1 / 305, 0.33%	1 / 13,714
chr2:g.154698981C>T	Substitution	Missense KCNJ3 S69L	1 / 305, 0.33%	1 / 13,714
chr2:g.154709704C>T	Substitution	Synonymous KCNJ3 L268=	1 / 305, 0.33%	1 / 13,714
chr2:g.154699449C>T	Substitution	Missense KCNJ3 S225F	1 / 305, 0.33%	1 / 13,714
chr2:g.154698901G>C	Substitution	Missense KCNJ3 K42N	1 / 305, 0.33%	1 / 13,714
chr2:g.154855044C>T	Substitution	Missense KCNJ3 P413S	1 / 305, 0.33%	1 / 13,714
chr2:g.154709812A>T	Substitution	Missense KCNJ3 E304D	1 / 305, 0.33%	1 / 13,714
chr2:g.154699216C>G	Substitution	Synonymous KCNJ3 G147=	1 / 305, 0.33%	1 / 13,714
chr2:g.154855008T>A	Substitution	Missense KCNJ3 S401T	1 / 305, 0.33%	1 / 13,714
chr2:g.154699019T>C	Substitution	Missense KCNJ3 W82R	1 / 305, 0.33%	1 / 13,714
chr2:g.154854965G>A	Substitution	Synonymous KCNJ3 V386=	1 / 305, 0.33%	1 / 13,714
chr2:g.154698938G>C	Substitution	Missense KCNJ3 V55L	1 / 305, 0.33%	1 / 13,714
chr2:g.154699246G>T	Substitution	Missense KCNJ3 E157D	1 / 305, 0.33%	1 / 13,714
chr2:g.154698872C>G	Substitution	Missense KCNJ3 P33A	1 / 305, 0.33%	1 / 13,714
chr2:g.154855139G>C	Substitution	Synonymous KCNJ3 P444=	1 / 305, 0.33%	1 / 13,714
chr2:g.154699143G>C	Substitution	Missense KCNJ3 C123S	1 / 305, 0.33%	1 / 13,714
chr2:g.154699221G>C	Substitution	Missense KCNJ3 R149P	1 / 305, 0.33%	1 / 13,714
chr2:g.154709780G>A	Substitution	Missense KCNJ3 E294K	1 / 305, 0.33%	1 / 13,714
chr2:g.154855024T>G	Substitution	Missense KCNJ3 I406S	1 / 305, 0.33%	1 / 13,714
chr2:g.154709701_154709702insCT CACAA	Insertion	Frameshift KCNJ3 I270Tfs*15	1 / 305, 0.33%	1 / 13,714

chr2:g.154699090C>G	Substitution	Missense KCNJ3 I105M	1 / 305, 0.33%	1 / 13,714
chr2:g.154854850C>T	Substitution	Missense KCNJ3 T348I	1 / 305, 0.33%	1 / 13,714
chr2:g.154854765G>T	Substitution	Stop Gained KCNJ3 E320*	1 / 305, 0.33%	1 / 13,714
chr2:g.154854776G>T	Substitution	Missense KCNJ3 W323C	1 / 305, 0.33%	1 / 13,714
chr2:g.154854943G>A	Substitution	Missense KCNJ3 S379N	1 / 305, 0.33%	1 / 13,714
chr2:g.154854882A>T	Substitution	Stop Gained KCNJ3 K359*	1 / 305, 0.33%	1 / 13,714
chr2:g.154699247G>A	Substitution	Missense KCNJ3 G158S	1 / 305, 0.33%	1 / 13,714
chr2:g.154709759A>T	Substitution	Missense KCNJ3 S287C	1 / 305, 0.33%	1 / 13,714
chr2:g.154855487G>A	Substitution	3 Prime UTR KCNJ3	1 / 305, 0.33%	1 / 13,714
chr2:g.154699256C>G	Substitution	Missense KCNJ3 L161V	1 / 305, 0.33%	1 / 13,714
chr2:g.154857025T>G	Substitution	3 Prime UTR KCNJ3	1 / 305, 0.33%	1 / 13,714
chr2:g.154699266T>A	Substitution	Missense KCNJ3 F164Y	1 / 305, 0.33%	1 / 13,714
chr2:g.154699237G>C	Substitution	Missense KCNJ3 K154N	1 / 305, 0.33%	1 / 13,714
chr2:g.154709737C>T	Substitution	Synonymous KCNJ3 P279=	1 / 305, 0.33%	1 / 13,714
chr2:g.154709795C>A	Substitution	Missense KCNJ3 L299I	1 / 305, 0.33%	1 / 13,714
chr2:g.154856896T>C	Substitution	3 Prime UTR KCNJ3	1 / 305, 0.33%	1 / 13,714
chr2:g.154699327G>A	Substitution	Missense KCNJ3 M184I	1 / 305, 0.33%	1 / 13,714
chr2:g.154699201C>T	Substitution	Synonymous KCNJ3 A142=	1 / 305, 0.33%	1 / 13,714
chr2:g.154698930G>T	Substitution	Missense KCNJ3 R52L	1 / 305, 0.33%	1 / 13,714
chr2:g.154709650A>T	Substitution	Missense KCNJ3 E250D	1 / 305, 0.33%	1 / 13,714
chr2:g.154699199G>A	Substitution	Missense KCNJ3 A142T	1 / 305, 0.33%	1 / 13,714
chr2:g.154855099G>A	Substitution	Missense KCNJ3 G431E	1 / 305, 0.33%	1 / 13,714
chr2:g.154854801T>C	Substitution	Missense KCNJ3 S332P	1 / 305, 0.33%	1 / 13,714
chr2:g.154698806G>A	Substitution	Missense KCNJ3 D11N	1 / 305, 0.33%	1 / 13,714
chr2:g.154709748T>G	Substitution	Missense KCNJ3 L283R	1 / 305, 0.33%	1 / 13,714
chr2:g.154699356T>A	Substitution	Missense KCNJ3 L194H	1 / 305, 0.33%	1 / 13,714
chr2:g.154699045C>T	Substitution	Synonymous KCNJ3 T90=	1 / 305, 0.33%	1 / 13,714
chr2:g.154699351G>A	Substitution	Synonymous KCNJ3 E192=	1 / 305, 0.33%	1 / 13,714
chr2:g.154854865C>A	Substitution	Missense KCNJ3 T353N	1 / 305, 0.33%	1 / 13,714
chr2:g.154855009C>G	Substitution	Missense KCNJ3 S401C	1 / 305, 0.33%	1 / 13,714
chr2:g.154855047delA	Deletion	Frameshift KCNJ3 K415Nfs*3	1 / 305, 0.33%	1 / 13,714
chr2:g.154699349G>A	Substitution	Missense KCNJ3 E192K	1 / 305, 0.33%	1 / 13,714
chr2:g.154855098G>A	Substitution	Missense KCNJ3 G431R	1 / 305, 0.33%	1 / 13,714
chr2:g.154709705A>T	Substitution	Missense KCNJ3 T269S	1 / 305, 0.33%	1 / 13,714
chr2:g.154854993A>G	Substitution	Missense KCNJ3 T396A	1 / 305, 0.33%	1 / 13,714
chr2:g.154698814G>A	Substitution	Synonymous KCNJ3 Q13=	1 / 305, 0.33%	1 / 13,714

chr2:g.154855022A>C	Substitution	Missense KCNJ3 K405N	1 / 305, 0.33%	1 / 13,714
chr2:g.154854837C>A	Substitution	Missense KCNJ3 Q344K	1 / 305, 0.33%	1 / 13,714
chr2:g.154854876A>G	Substitution	Missense KCNJ3 S357G	1 / 305, 0.33%	1 / 13,714
chr2:g.154854927C>A	Substitution	Missense KCNJ3 P374T	1 / 305, 0.33%	1 / 13,714
chr2:g.154699233delA	Deletion	Frameshift KCNJ3 D153Afs*49	1 / 305, 0.33%	1 / 13,714
chr2:g.154855192C>T	Substitution	Missense KCNJ3 P462L	1 / 305, 0.33%	1 / 13,714
chr2:g.154699452C>T	Substitution	Missense KCNJ3 A226V	1 / 305, 0.33%	1 / 13,714
chr2:g.154855199C>T	Substitution	Synonymous KCNJ3 S464=	1 / 305, 0.33%	1 / 13,714
chr2:g.154698895G>T	Substitution	Missense KCNJ3 K40N	1 / 305, 0.33%	1 / 13,714
chr2:g.154854953A>T	Substitution	Missense KCNJ3 R382S	1 / 305, 0.33%	1 / 13,714
chr2:g.154698875C>T	Substitution	Stop Gained KCNJ3 Q34*	1 / 305, 0.33%	1 / 13,714
chr2:g.154709662T>G	Substitution	Synonymous KCNJ3 G254=	1 / 305, 0.33%	1 / 13,714
chr2:g.154855180T>C	Substitution	Missense KCNJ3 M458T	1 / 305, 0.33%	1 / 13,714
chr2:g.154698888T>C	Substitution	Missense KCNJ3 V38A	1 / 305, 0.33%	1 / 13,714
chr2:g.154709723G>T	Substitution	Missense KCNJ3 D275Y	1 / 305, 0.33%	1 / 13,714
chr2:g.154698902C>T	Substitution	Missense KCNJ3 R43W	1 / 305, 0.33%	1 / 13,714
chr2:g.154855151A>G	Substitution	Synonymous KCNJ3 E448=	1 / 305, 0.33%	1 / 13,714
chr2:g.154709798G>C	Substitution	Missense KCNJ3 E300Q	1 / 305, 0.33%	1 / 13,714
chr2:g.154855132C>T	Substitution	Missense KCNJ3 S442L	1 / 305, 0.33%	1 / 13,714
chr2:g.154854958A>T	Substitution	Missense KCNJ3 N384I	1 / 305, 0.33%	1 / 13,714
chr2:g.154709672G>C	Substitution	Missense KCNJ3 G258R	1 / 305, 0.33%	1 / 13,714
chr2:g.154855161G>T	Substitution	Missense KCNJ3 V452L	1 / 305, 0.33%	1 / 13,714
chr2:g.154855038G>T	Substitution	Missense KCNJ3 D411Y	1 / 305, 0.33%	1 / 13,714
chr2:g.154699054G>T	Substitution	Synonymous KCNJ3 V93=	1 / 305, 0.33%	1 / 13,714
chr2:g.154709641C>T	Substitution	Synonymous KCNJ3 D247=	1 / 305, 0.33%	1 / 13,714
chr2:g.154857120T>G	Substitution	3 Prime UTR KCNJ3	1 / 305, 0.33%	1 / 13,714
chr2:g.154698814G>T	Substitution	Missense KCNJ3 Q13H	1 / 305, 0.33%	1 / 13,714
chr2:g.154699207C>A	Substitution	Synonymous KCNJ3 I144=	1 / 305, 0.33%	1 / 13,714
chr2:g.154699084G>T	Substitution	Missense KCNJ3 W103C	1 / 305, 0.33%	1 / 13,714
chr2:g.154858342T>C	Substitution	3 Prime UTR KCNJ3	1 / 305, 0.33%	1 / 13,714
chr2:g.154855083A>C	Substitution	Missense KCNJ3 K426Q	1 / 305, 0.33%	1 / 13,714
chr2:g.154854969T>A	Substitution	Missense KCNJ3 C388S	1 / 305, 0.33%	1 / 13,714
chr2:g.154698948G>T	Substitution	Missense KCNJ3 G58V	1 / 305, 0.33%	1 / 13,714
chr2:g.154854814delGATTCTTTAAAGTT	Deletion	Frameshift KCNJ3 F337Lfs*9	1 / 305, 0.33%	1 / 13,714
chr2:g.154699440A>G	Substitution	Missense KCNJ3 H222R	1 / 305, 0.33%	1 / 13,714
chr2:g.154855277_154855278insA	Insertion	Frameshift KCNJ3 L492Ifs*7	1 / 305, 0.33%	1 / 13,714

chr2:g.154855043T>C	Substitution	Synonymous KCNJ3 F412=	1 / 305, 0.33%	1 / 13,714
chr2:g.154698999T>G	Substitution	Missense KCNJ3 L75R	1 / 305, 0.33%	1 / 13,714
chr2:g.154855269C>A	Substitution	Missense KCNJ3 L488I	1 / 305, 0.33%	1 / 13,714
chr2:g.154856286T>C	Substitution	3 Prime UTR KCNJ3	1 / 305, 0.33%	1 / 13,714
chr2:g.154709748T>C	Substitution	Missense KCNJ3 L283P	1 / 305, 0.33%	1 / 13,714
chr2:g.154698895G>C	Substitution	Missense KCNJ3 K40N	1 / 305, 0.33%	1 / 13,714
chr2:g.154855178G>A	Substitution	Synonymous KCNJ3 K457=	1 / 305, 0.33%	1 / 13,714
chr2:g.154709712G>A	Substitution	Missense KCNJ3 C271Y	1 / 305, 0.33%	1 / 13,714
chr2:g.154698829G>A	Substitution	Synonymous KCNJ3 S18=	1 / 305, 0.33%	1 / 13,714
chr2:g.154699124G>T	Substitution	Missense KCNJ3 V117F	1 / 305, 0.33%	1 / 13,714
chr2:g.154709673G>A	Substitution	Missense KCNJ3 G258E	1 / 305, 0.33%	1 / 13,714
chr2:g.154698948G>A	Substitution	Missense KCNJ3 G58D	1 / 305, 0.33%	1 / 13,714
chr2:g.154699183C>A	Substitution	Missense KCNJ3 F136L	1 / 305, 0.33%	1 / 13,714
chr2:g.154855128A>C	Substitution	Missense KCNJ3 S441R	1 / 305, 0.33%	1 / 13,714
chr2:g.154855095T>G	Substitution	Missense KCNJ3 L430V	1 / 305, 0.33%	1 / 13,714
chr2:g.154699306C>T	Substitution	Synonymous KCNJ3 I177=	1 / 305, 0.33%	1 / 13,714
chr2:g.154699209G>C	Substitution	Missense KCNJ3 G145A	1 / 305, 0.33%	1 / 13,714
chr2:g.154698983G>A	Substitution	Missense KCNJ3 D70N	1 / 305, 0.33%	1 / 13,714
chr2:g.154858184T>G	Substitution	3 Prime UTR KCNJ3	1 / 305, 0.33%	1 / 13,714
chr2:g.154709761C>A	Substitution	Missense KCNJ3 S287R	1 / 305, 0.33%	1 / 13,714
chr2:g.154854860C>T	Substitution	Synonymous KCNJ3 V351=	1 / 305, 0.33%	1 / 13,714
chr2:g.154698982G>A	Substitution	Synonymous KCNJ3 S69=	1 / 305, 0.33%	1 / 13,714
chr2:g.154698845T>C	Substitution	Synonymous KCNJ3 L24=	1 / 305, 0.33%	1 / 13,714
chr2:g.154854793C>T	Substitution	Missense KCNJ3 P329L	1 / 305, 0.33%	1 / 13,714
chr2:g.154699051C>T	Substitution	Synonymous KCNJ3 T92=	1 / 305, 0.33%	1 / 13,714
chr2:g.154854777G>T	Substitution	Missense KCNJ3 G324C	1 / 305, 0.33%	1 / 13,714
chr2:g.154699190G>A	Substitution	Missense KCNJ3 E139K	1 / 305, 0.33%	1 / 13,714
chr2:g.154698946C>T	Substitution	Synonymous KCNJ3 H57=	1 / 305, 0.33%	1 / 13,714
chr2:g.154699138G>A	Substitution	Synonymous KCNJ3 T121=	1 / 305, 0.33%	1 / 13,714
chr2:g.154699395G>T	Substitution	Missense KCNJ3 G207V	1 / 305, 0.33%	1 / 13,714
chr2:g.154698988C>T	Substitution	Synonymous KCNJ3 L71=	1 / 305, 0.33%	1 / 13,714
chr2:g.154699127G>C	Substitution	Missense KCNJ3 G118R	1 / 305, 0.33%	1 / 13,714
chr2:g.154699330C>A	Substitution	Synonymous KCNJ3 S185=	1 / 305, 0.33%	1 / 13,714
chr2:g.154854883A>T	Substitution	Missense KCNJ3 K359I	1 / 305, 0.33%	1 / 13,714
chr2:g.154855184A>T	Substitution	Missense KCNJ3 L459F	1 / 305, 0.33%	1 / 13,714
chr2:g.154855251G>A	Substitution	Missense KCNJ3 A482T	1 / 305, 0.33%	1 / 13,714

chr2:g.154855096T>C	Substitution	Missense KCNJ3 L430S	1 / 305, 0.33%	1 / 13,714
chr2:g.154855066G>A	Substitution	Missense KCNJ3 S420N	1 / 305, 0.33%	1 / 13,714
chr2:g.154699137C>T	Substitution	Missense KCNJ3 T121M	1 / 305, 0.33%	1 / 13,714
chr2:g.154858009C>T	Substitution	3 Prime UTR KCNJ3	1 / 305, 0.33%	1 / 13,714
chr2:g.154709699C>A	Substitution	Missense KCNJ3 P267T	1 / 305, 0.33%	1 / 13,714
chr2:g.154854782T>C	Substitution	Synonymous KCNJ3 H325=	1 / 305, 0.33%	1 / 13,714
chr2:g.154698825C>T	Substitution	Missense KCNJ3 T17I	1 / 305, 0.33%	1 / 13,714
chr2:g.154855246G>T	Substitution	Missense KCNJ3 G480V	1 / 305, 0.33%	1 / 13,714
chr2:g.154855247A>T	Substitution	Synonymous KCNJ3 G480=	1 / 305, 0.33%	1 / 13,714
chr2:g.154709727C>T	Substitution	Missense KCNJ3 A276V	1 / 305, 0.33%	1 / 13,714
chr2:g.154699170C>A	Substitution	Missense KCNJ3 S132Y	1 / 305, 0.33%	1 / 13,714
chr2:g.154698780C>T	Substitution	Missense KCNJ3 S2F	1 / 305, 0.33%	1 / 13,714
chr2:g.154855307C>T	Substitution	Synonymous KCNJ3 F500=	1 / 305, 0.33%	1 / 13,714
chr2:g.154857921A>T	Substitution	3 Prime UTR KCNJ3	1 / 305, 0.33%	1 / 13,714
chr2:g.154855081delA	Deletion	Frameshift KCNJ3 A427Pfs*9	1 / 305, 0.33%	1 / 13,714
chr2:g.154709664T>A	Substitution	Missense KCNJ3 F255Y	1 / 305, 0.33%	1 / 13,714
chr2:g.154698930G>A	Substitution	Missense KCNJ3 R52Q	1 / 305, 0.33%	1 / 13,714
chr2:g.154856628G>A	Substitution	3 Prime UTR KCNJ3	1 / 305, 0.33%	1 / 13,714
chr2:g.154709620G>A	Substitution	Synonymous KCNJ3 E240=	1 / 305, 0.33%	1 / 13,714
chr2:g.154699295G>A	Substitution	Missense KCNJ3 A174T	1 / 305, 0.33%	1 / 13,714
chr2:g.154709681C>T	Substitution	Stop Gained KCNJ3 Q261*	1 / 305, 0.33%	1 / 13,714
chr2:g.154699060G>A	Substitution	Stop Gained KCNJ3 W95*	1 / 305, 0.33%	1 / 13,714
chr2:g.154699051C>A	Substitution	Synonymous KCNJ3 T92=	1 / 305, 0.33%	1 / 13,714
chr2:g.154709813A>G	Substitution	Missense KCNJ3 T305A	1 / 305, 0.33%	1 / 13,714
chr2:g.154709820G>C	Substitution	Splice Donor KCNJ3 X307_splice	1 / 305, 0.33%	1 / 13,714
chr2:g.154698805C>T	Substitution	Synonymous KCNJ3 D10=	1 / 305, 0.33%	1 / 13,714
chr2:g.154699402C>A	Substitution	Synonymous KCNJ3 L209=	1 / 305, 0.33%	1 / 13,714
chr2:g.154854995T>C	Substitution	Synonymous KCNJ3 T396=	1 / 305, 0.33%	1 / 13,714
chr2:g.154699292G>A	Substitution	Missense KCNJ3 D173N	1 / 305, 0.33%	1 / 13,714
chr2:g.154709696_154709697insC	Insertion	Frameshift KCNJ3 L268Pfs*15	1 / 305, 0.33%	1 / 13,714
chr2:g.154698857G>T	Substitution	Missense KCNJ3 G28W	1 / 305, 0.33%	1 / 13,714
chr2:g.154699430C>T	Substitution	Missense KCNJ3 R219C	1 / 305, 0.33%	1 / 13,714
chr2:g.154854984G>T	Substitution	Missense KCNJ3 D393Y	1 / 305, 0.33%	1 / 13,714
chr2:g.154699365G>A	Substitution	Missense KCNJ3 S197N	1 / 305, 0.33%	1 / 13,714
chr2:g.154698927G>A	Substitution	Missense KCNJ3 G51D	1 / 305, 0.33%	1 / 13,714
chr2:g.154699127G>A	Substitution	Missense KCNJ3 G118S	1 / 305, 0.33%	1 / 13,714

chr2:g.154698788C>T	Substitution	Stop Gained KCNJ3 R5*	1 / 305, 0.33%	1 / 13,714
chr2:g.154699228C>T	Substitution	Synonymous KCNJ3 I151=	1 / 305, 0.33%	1 / 13,714

From: (Pelzmann, Hatab et al. 2022).

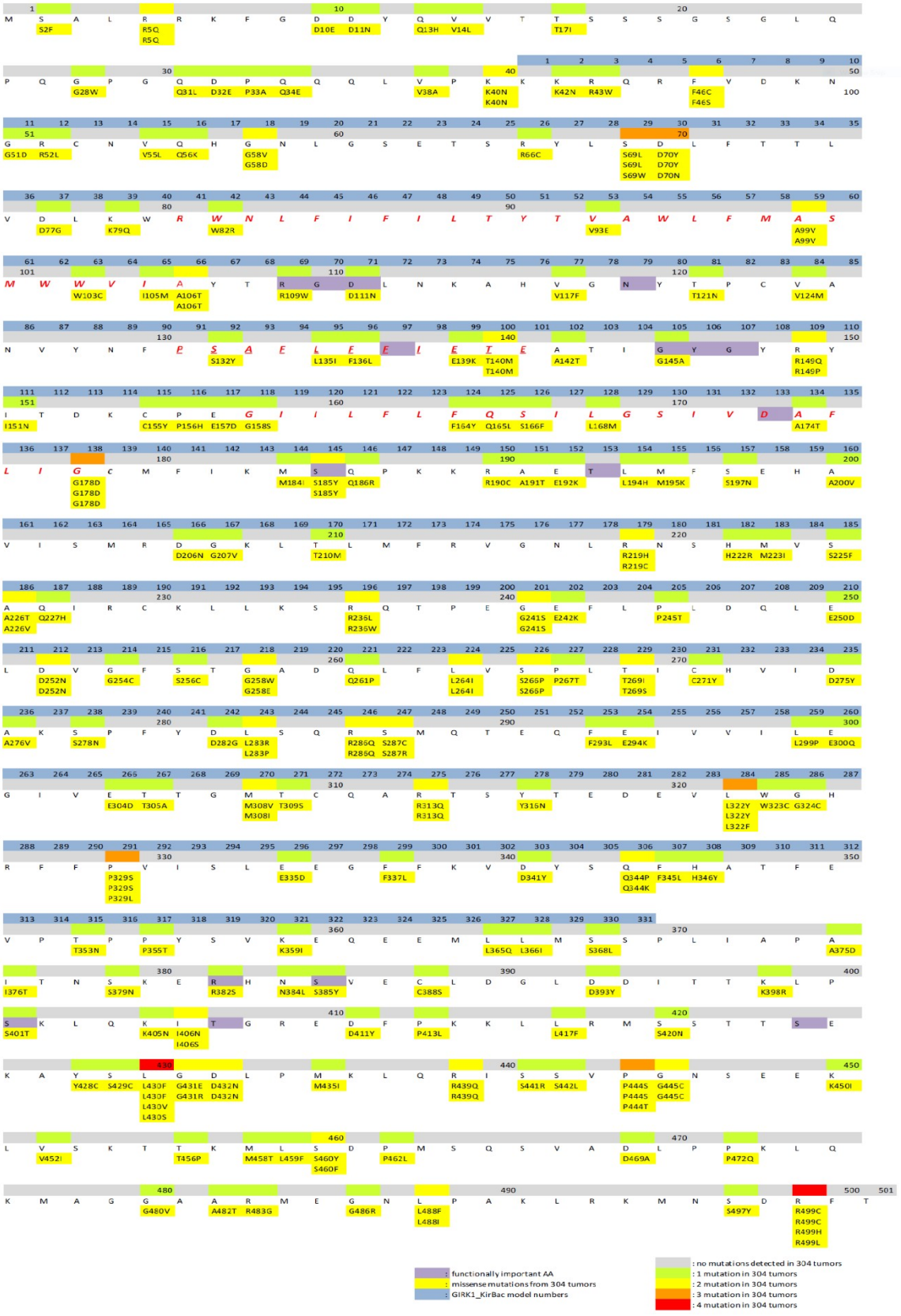

Figure 17: Location of all detected missense mutations in the primary structure of the GIRK1 subunit. Somatic mutations in the GIRK1 subunit: Amino acid numbering according to entire full length variant 1a. Regions comprising the pore helix and the transmembrane helix 2 are emphasized in red. Somatic mutations detected are highlighted in green 1 mutation found, yellow 2 mutations found, orange 3 mutations found and red 4 mutations found out of 304 cases. Multiple appearance of a mutation underneath an amino acid residue

indicates multiple occurrences in different tumors of the sample cohort. Numbers in blue boxes: Amino acid numbering of KirBac structure according to (Nishida, Cadene et al. 2007).

From: (Pelzmann, Hatab et al. 2022).

Table 4: Statistical data and numerical figures for Quantitative expression of GIRK1 subunit mutations.

	ΔF mean	SEM	N	p-value (vs. natives)	p-value (Mutant vs. WT)	p-value (-G4 vs. +G4)
native	0,01	0,00	109			
WT	0,28	0,03	136	< 0,001		< 0,001
WT+G4	1,00	0,04	142	< 0,001		
S132Y	0,21	0,03	25	< 0,001	0,468	< 0,001
S132Y+G4	0,66	0,08	24	< 0,001	0,007	
L135I	0,20	0,03	25	< 0,001	0,135	< 0,001
L135I+G4	0,77	0,12	23	< 0,001	0,729	
F136L	0,28	0,06	19	0,060	> 0,999	< 0,001
F136L+G4	0,65	0,11	20	0,015	0,007	
E139K	0,26	0,03	19	< 0,001	> 0,999	< 0,001
E139K+G4	1,00	0,13	19	< 0,001	> 0,999	
E140M	0,11	0,02	14	0,045	< 0,001	< 0,001
E140M+G4	1,00	0,12	14	< 0,001	0,830	
A142T	0,43	0,08	23	0,060	0,748	< 0,001
A142T+G4	2,48	0,35	19	< 0,001	0,055	
G145A	0,32	0,08	23	0,072	> 0,999	0,015
G145A+G4	0,66	0,13	24	0,045	0,570	
R149Q	0,23	0,02	24	< 0,001	0,748	< 0,001
R149Q+G4	1,36	0,33	24	0,101	> 0,999	
R149P	0,36	0,08	24	0,052	> 0,999	< 0,001
R149P+G4	1,12	0,24	23	0,060	> 0,999	
I151N	0,13	0,02	28	0,008	< 0,001	0,503
I151N+G4	0,29	0,09	29	0,015	< 0,001	
G158S	0,11	0,02	27	< 0,001	< 0,001	0,393
G158S+G4	0,15	0,06	29	0,262	< 0,001	
G178D	0,14	0,02	24	0,015	< 0,001	< 0,001
G178D+G4	1,28	0,18	24	< 0,001	0,830	
M184I	0,23	0,03	20	0,024	0,748	0,004
M184I+G4	0,99	0,10	17	0,101	> 0,999	
S185Y	0,17	0,03	23	0,024	0,072	< 0,001
S185Y+G4	1,23	0,13	24	< 0,001	0,830	
Q186R	0,29	0,04	22	< 0,001	> 0,999	< 0,001
Q186R+G4	1,67	0,24	19	< 0,001	0,729	

Note: Values with red text highlight statistically significant values.

From: (Pelzmann, Hatab et al. 2022).

Table 5: Statistical data and numerical figures for I_{ACh}/I_{total} ratios.

	I_{ACh}/I_{total} (mean)	SEM	N	p-value (mutant vs. WT)
WT	0,42	0,01	137	
S132Y	0,42	0,03	24	> 0,999
L135I	0,37	0,03	23	0,980
F136L	0,42	0,03	25	> 0,999
E139K	0,43	0,03	24	> 0,999
E140M	0,31	0,04	23	0,143
A142T	0,42	0,03	20	> 0,999
G145A	0,34	0,03	23	0,234
R149Q	0,43	0,04	25	> 0,999
R149P	0,38	0,04	23	> 0,999
I151N	0,51	0,02	24	0,049
G158S	0,49	0,03	29	0,237
G178D	0,37	0,02	25	> 0,999
M184I	0,46	0,03	15	> 0,999
S185Y	0,28	0,02	24	< 0,001
Q186R	0,44	0,03	23	> 0,999

Note: Values with red text highlight statistically significant values.

From: (Pelzmann, Hatab et al. 2022).

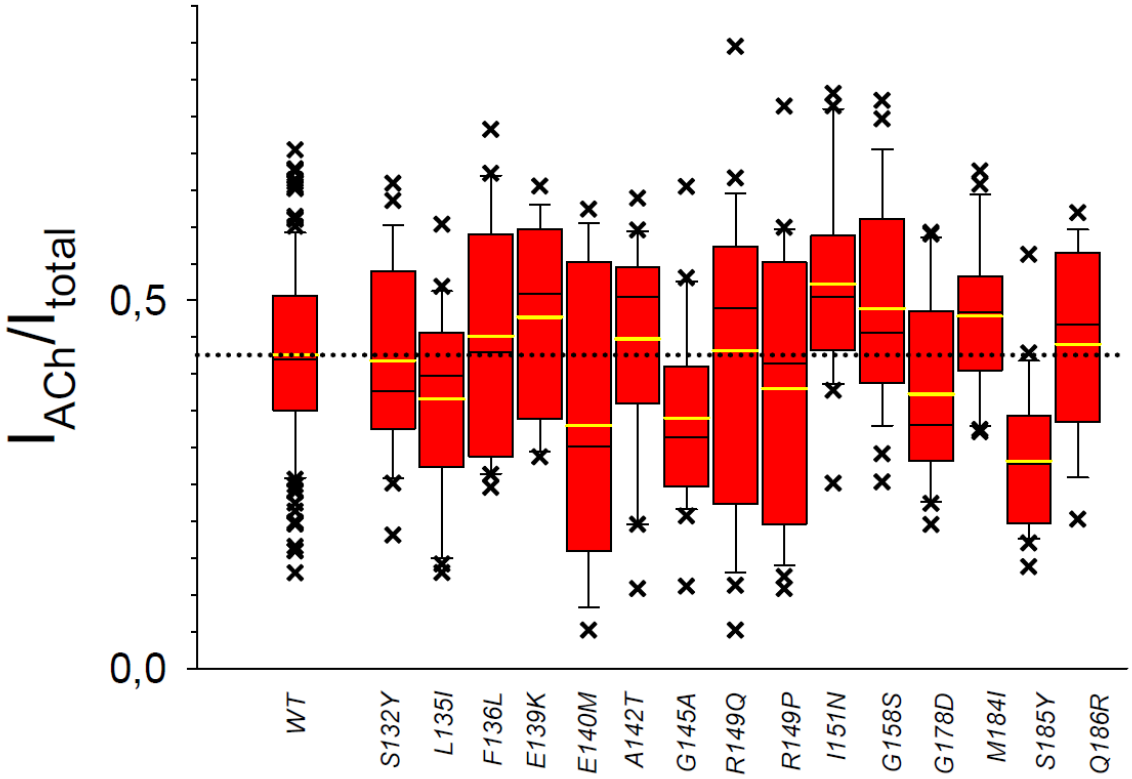

Figure 18: Various GIRK1^{eGFP} subunit mutations' I_{ACh}/I_{total} ratios in comparison to WT

GIRK1 and GIRK4 mRNA were co-injected. Percentiles of 25% and 75% are included in box plots. A box with a yellow line indicating the average value and a solid black line as the median. Whiskers indicate percentiles of 10% and 90%. Oocytes with values above and below the 90% and 10% percentile rank are shown by a cross. The dotted line represents the median WT/GIRK4 value. From: (Pelzmann, Hatab et al. 2022).

Table 6: Values and statistics of total current amplitudes, produced by different GIRK1^{eGFP} subunit mutations, relative to GIRK1^{WT}/GIRK4 channels.

	I_{total} mean	SEM	N	p-value (vs. natives)	p-value (Mutant vs. WT)	p-value (-G4 vs. +G4)
native	0,02	0,00	109			
G4 (homo)	0,20	0,02	130	< 0,001		
WT	0,07	0,00	133	< 0,001		< 0,001
WT+G4	1,00	0,03	137	< 0,001		
S132Y	0,03	0,01	25	0,635	< 0,001	< 0,001
S132Y+G4	0,57	0,07	24	0,004	< 0,001	
L135I	0,04	0,00	25	0,012	< 0,001	< 0,001
L135I+G4	0,95	0,10	23	< 0,001	0,649	
F136L	0,02	0,00	24	> 0,999	< 0,001	< 0,001
F136L+G4	0,72	0,07	25	< 0,001	< 0,001	
E139K	0,02	0,01	25	> 0,999	< 0,001	< 0,001
E139K+G4	0,21	0,04	24	> 0,999	< 0,001	
E140M	0,03	0,00	24	> 0,999	< 0,001	< 0,001
E140M+G4	1,22	0,13	23	< 0,001	0,252	
A142T	0,10	0,01	20	< 0,001	0,034	< 0,001
A142T+G4	1,31	0,14	20	< 0,001	0,166	
G145A	0,03	0,00	24	> 0,999	< 0,001	< 0,001
G145A+G4	0,32	0,09	23	0,678	< 0,001	
R149Q	0,02	0,00	24	> 0,999	< 0,001	< 0,001
R149Q+G4	0,71	0,09	25	< 0,001	0,039	
R149P	0,02	0,00	24	> 0,999	< 0,001	< 0,001
R149P+G4	0,72	0,12	23	0,018	0,166	
I151N	0,02	0,00	23	> 0,999	< 0,001	< 0,001
I151N+G4	0,42	0,09	24	0,480	< 0,001	
G158S	0,02	0,00	27	> 0,999	< 0,001	< 0,001
G158S+G4	0,21	0,03	29	> 0,999	< 0,001	
G178D	0,04	0,01	25	0,535	< 0,001	< 0,001
G178D+G4	0,68	0,06	25	< 0,001	< 0,001	
M184I	0,13	0,01	16	< 0,001	< 0,001	< 0,001
M184I+G4	1,63	0,22	15	< 0,001	0,093	
S185Y	0,03	0,00	23	0,479	< 0,001	< 0,001
S185Y+G4	0,27	0,03	24	0,480	< 0,001	
Q186R	0,05	0,00	24	< 0,001	< 0,001	< 0,001
Q186R+G4	0,43	0,07	23	0,039	< 0,001	

Note: Values with red text highlight statistically significant values.

From: (Pelzmann, Hatab et al. 2022).